LEVEL

⑫

AD A102344

FINAL TECHNICAL REPORT

FRACTURE AND FATIGUE OF BI-MATERIALS

F49620-80-C-0010

Period 1 December 1979 to 30 November 1980

MIT OSP 88845

Reported by James W. Mar
Jerome C. Hunsaker Professor
of Aerospace Education

TABLE OF CONTENTS

REPORT DOCUMENTATION PAGE	READ INSTRUCTIONS BEFORE COMPLETING FORM

1. REPORT NUMBER AFOSR-TR—81-0596	2. GOVT ACCESSION NO. AD-A02 344	3. RECIPIENT'S CATALOG NUMBER

4. TITLE (and Subtitle) FRACTURE AND FATIGUE OF BI-MATERIALS	5. TYPE OF REPORT & PERIOD COVERED FINAL 1 Dec 79-30 Nov 80
	6. PERFORMING ORG. REPORT NUMBER

7. AUTHOR(s) JAMES W. MAR JEROME C. HUNSAKER	8. CONTRACT OR GRANT NUMBER(s) F49620-80-C-0010

9. PERFORMING ORGANIZATION NAME AND ADDRESS MASSACHUSETTS INSTITUTE OF TECHNOLOGY CAMBRIDGE, MA 02139	10. PROGRAM ELEMENT, PROJECT, TASK AREA & WORK UNIT NUMBERS 2307/B1 61102F

11. CONTROLLING OFFICE NAME AND ADDRESS AIR FORCE OFFICE OF SCIENTIFIC RESEARCH/NA BUILDING 410 BOLLING AFB, DC 20332	12. REPORT DATE NOV 80
	13. NUMBER OF PAGES 110

14. MONITORING AGENCY NAME & ADDRESS(if different from Controlling Office)	15. SECURITY CLASS. (of this report) UNCLASSIFIED
	15a. DECLASSIFICATION DOWNGRADING SCHEDULE

16. DISTRIBUTION STATEMENT (of this Report)

Approved for public release; distribution unlimited.

17. DISTRIBUTION STATEMENT (of the abstract entered in Block 20, if different from Report)

18. SUPPLEMENTARY NOTES

19. KEY WORDS (Continue on reverse side if necessary and identify by block number)

FATIGUE LIFE
RESIDUAL STRENGTH
DELAMINATION
LAMINATE
LAYUP

20. ABSTRACT (Continue on reverse side if necessary and identify by block number)

Eighty-nine axially loaded, aluminum honeycomb sandwich specimens with graphite/epoxy face sheets of four different laminates were compressively cycled with a minimum to maximum load ratio of R=10. Fatigue damage initiation and propagation were monitored on both graphite/epoxy faces of each specimen using Moire interferometry, a method of optically producing surface contour lines. These patterns were photographically recorded at intervals for later analysis. Life, residual strength, cycles to damage initiation and damage growth data are

DD FORM 1473 EDITION OF 1 NOV 65 IS OBSOLETE

reported. Damage initiation site and mode are compared with the analytically predicted three dimensional stress field at the edge of the hole. The location of first observable damage in all laminates was an experimentally repeatable layup characteristic. All laminate types showed a nearly horizontal initial region of damage growth followed by a second region of gradually increasing damage area growth with loading cycles, and a final region of very rapid growth just prior to failure. Post fatigue inspection showed damage concentrated mainly in the angle plys. No well defined relationship could be established however, between specimen fracture and final damage area. Life to first damage and life to specimen failure for the four laminate types showed that both stacking sequence and ply orientation had an affect on the response of a specimen to cyclic compression loads.

SUMMARY OF MAJOR FINDINGS

I.   Fracture of $[0_2/\pm\theta]_s$ Laminates with a 6.35 mm Diameter Hole
──

1.1   Eight ply $[0_2/\pm\theta]_s$ laminates were fabricated into tensile coupons
       each containing a 6.35 mm diameter hole. The cross-ply angles,
       θ, were 15, 30, 45, 60, 75, and 90 degrees. There were five
       specimens for each angle θ. Figure 1 shows the nominal dimen-
       sions of the coupon type of specimen used in these investigations.

1.2   The ultimate stresses are shown in Figure 2 and the ultimate
       strains measured at fracture are shown in Figure 3.

1.3   It is seen from Figures 2 and 3 that the laminates $[0_2/\pm30]_s$
       exhibit two distinct levels of behavior. One group (3 specimens)
       failed at an appreciably lower fracture stress and ultimate strain
       than the other group (2 specimens). As can be seen, the ultimate
       stresses versus θ are aligned into two distinct curves with a
       marked discontinuity at $\theta=30°$. The ultimate strains versus θ
       are similarly aligned.

1.4   The stress-strain curves for the specimens with θ less than 30°
       are essentially linear to failure whereas for the specimens with
       θ greater than 30° the stress-strain curves are essentially
       bilinear (see Figure 4) to failure. For the specimens of
       laminate $[0_2/\pm30]_s$, the three specimens which failed at higher
       stress exhibited the bilinear form of stress-strain behavior
       while the other two, which failed at lower stress, were
       linear to failure.

II. Crack Growth of Splits in Uni-directional Laminates with a Hole

2.1 In an earlier investigation the splitting of uni-directional laminates containing a hole caused by the static (one-time) application of tensile loads was investigated. In this research 4-ply uni-directional laminates containing a 3.2 mm (.125 inch) diameter hole were cyclically loaded at constant amplitude to determine the growth of the split with the number of cycles. Seventeen specimens were cycled between 8% and 80% of the nominal splitting stress of 330 MPa. Three specimens were cycled between 7% and 70%, and four were cycled between 6% and 60%. Most tests were terminated at 50,000 cycles with a few being continued to 500,000 cycles.

2.2 Typical crack length vs. cycle data is shown in Figure 5. The splits do not initiate symmetrically from the edge of the hole and as indicated in Figure 5, the splits are located relative to the hole in four locations. The curve labeled T is the sum of the lengths labeled 1 and 2 where B is the sum of 3 and 4.

2.3 The crack growth data has been fitted to the equation

$$2a = A \log N - K$$

where

    2a   is the total crack length

    N   is the number of cycles

'A' and 'K' are constants that depend upon the cyclic stress levels. This equation was used to extrapolate backwards to N_0, the number of cycles for crack initiation.

2.4 The values of F, K and N_0 for the three cyclic load levels are shown in Table IV. It should be remembered that the number of specimens for two smallest load levels are quite small.

III. Static Tensile Behavior of $[0/\pm\theta]_s$ and $[\pm\theta/0]_s$ Laminates with Holes

3.1 This research experimentally determined the fracture behavior of specimens containing various sized holes in the laminate systems $[0/\pm\theta]_s$ and $[\pm\theta/0]_s$ with $\theta=0$, 5, 10 and 15 degrees. Tables V and VI summarize the testing program.

3.2 The fracture, i.e. failure, stresses for all the specimens are summarized in Tables VII through XVI.

3.3 The effect of hole size on the fracture strength has been correlated against the relation

$$\sigma_f = H_c(2a)^{-m}$$

where
2a   is the hole diameter in millimeters

H_c is a "composite toughness" with dimensions $MPa(mm)^m$

and   m   is a parameter analogous to the factor of .5 (the singularity) in linear elastic fracture mechanics.

Table XVI summarizes the value of H_c and m obtained in these investigations.

IV. Damage Initiation and Propagation During Compressive Fatigue of Flawed Graphite/Epoxy Composites

4.1 Compression-compression fatigue tests of four different graphite/ epoxy layups, $(\pm 45/0)_s$, $(0/\pm 45)_s$, $(\pm 30/0)_s$ and $(0/\pm 30)_s$, have been conducted. Buckling of these axially loaded laminates was prevented by the use of a sandwich specimen composed of a 2.5 cm. thick aluminum honeycomb core faced with two 5x30.5 cm. G/E coupons. Damage initiation and propagation near the 1.25 cm. diameter hole in each G/E face sheet was monitored and recorded during testing. Inspection of the laminates was by Moire inter- ferometry, a method of optically producing a visible contour map of the small out-of-plane surface displacements resulting from subsurface delamination. Specimen cross sections were microscopically examined to compare the observed Moire patterns with the actual damage developed during cyclic loading.

4.2 A comprehensive set of damage progression photographs are presented. These pictures, along with plots of damage area growth, show that each of the four laminate types displays its own characteristic pattern of initiation and propagation. No well defined relationship between specimen fracture and final damage area was observed, however, the rapid growth of damage

prior to failure *usually provided some warning that fracture was* imminent. Life to first damage and life to specimen failure for the four laminate types showed that both stacking sequence and ply orientation can affect the response of a specimen to cyclic compression loads.

4.3 It is difficult at this time to easily summarize all the results of this investigation. There is included as Appendix A excerpts taken from the fall report.

TOP VIEW **SIDE VIEW**

75 mm — GLASS/EPOXY TAB

30°

200 mm — GRAPHITE/EPOXY

GRAPHITE/EPOXY

FM-123 FILM ADHESIVE

GLASS/EPOXY

75 mm

GLASS/EPOXY
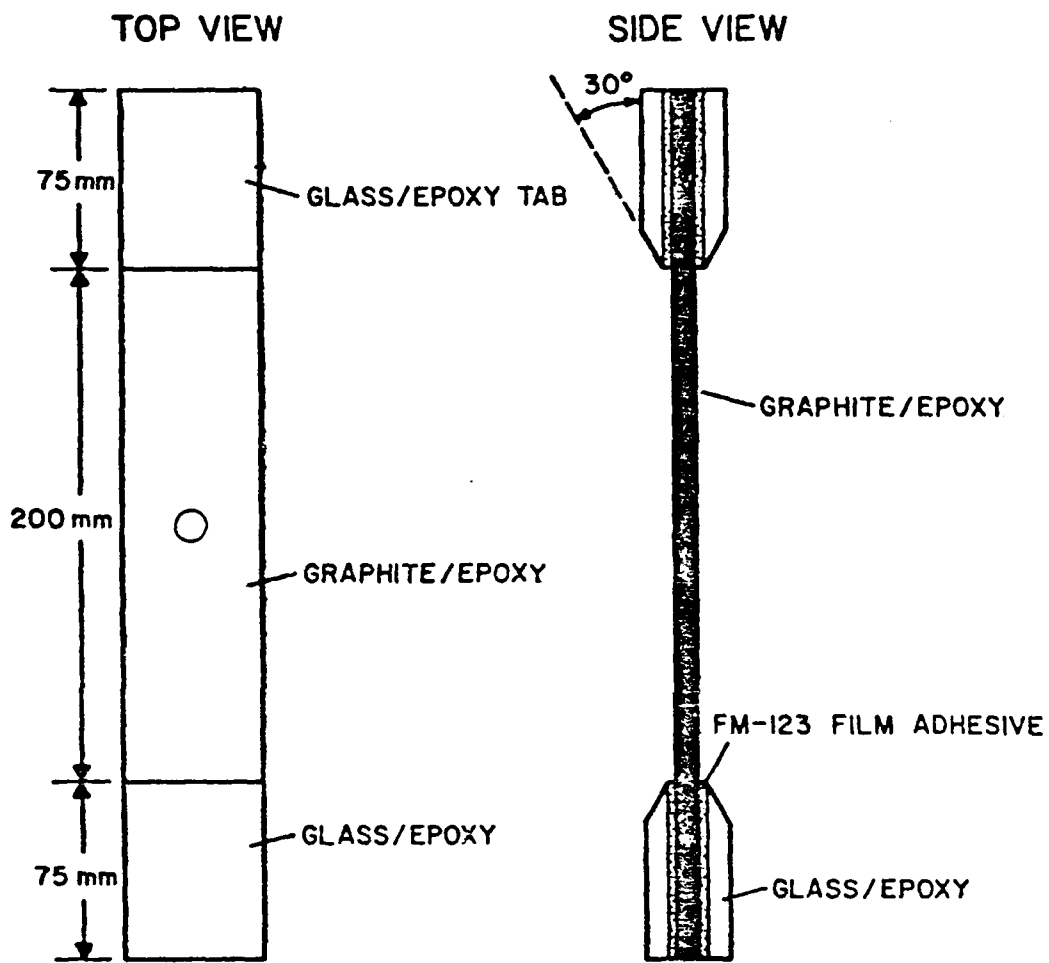
FIG. 1:   THE PHYSICAL CHARACTERISTICS OF THE
COUPON SPECIMEN

FIGURE 2
FRACTURE OF $[0_2/\pm\theta]_s$ LAMINATE WITH A HOLE
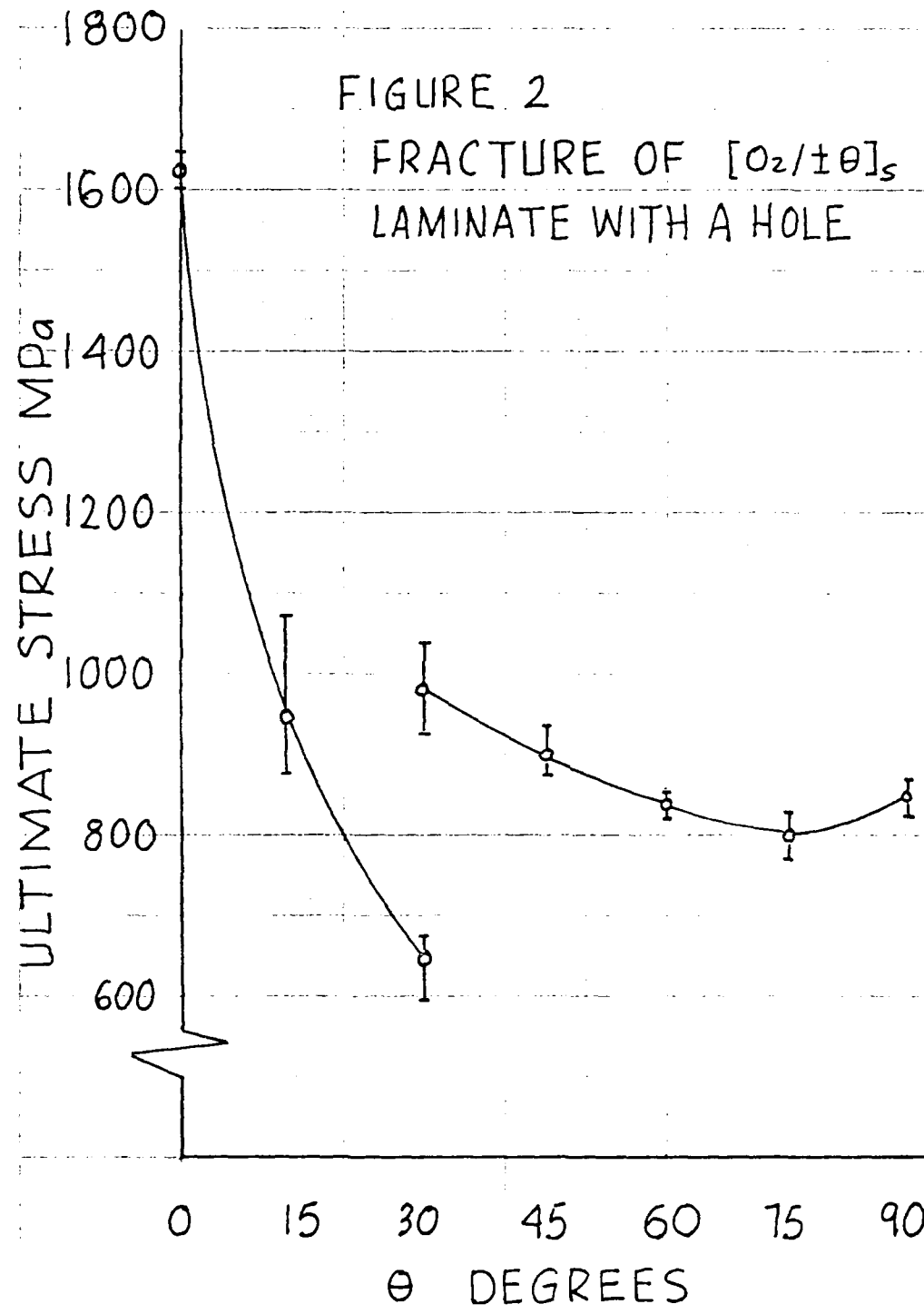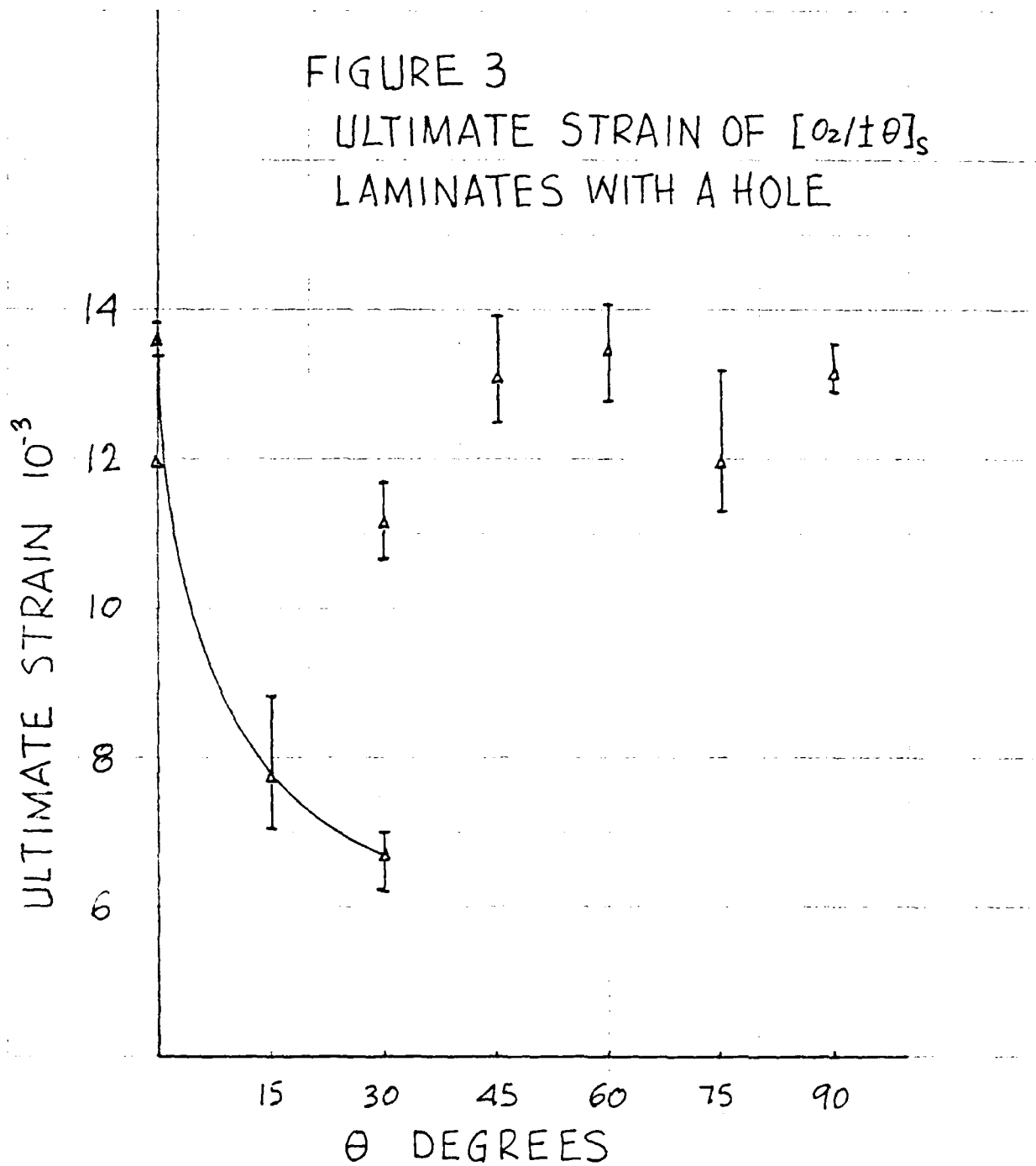
FIGURE 3
ULTIMATE STRAIN OF $[0_2/\pm\theta]_s$
LAMINATES WITH A HOLE
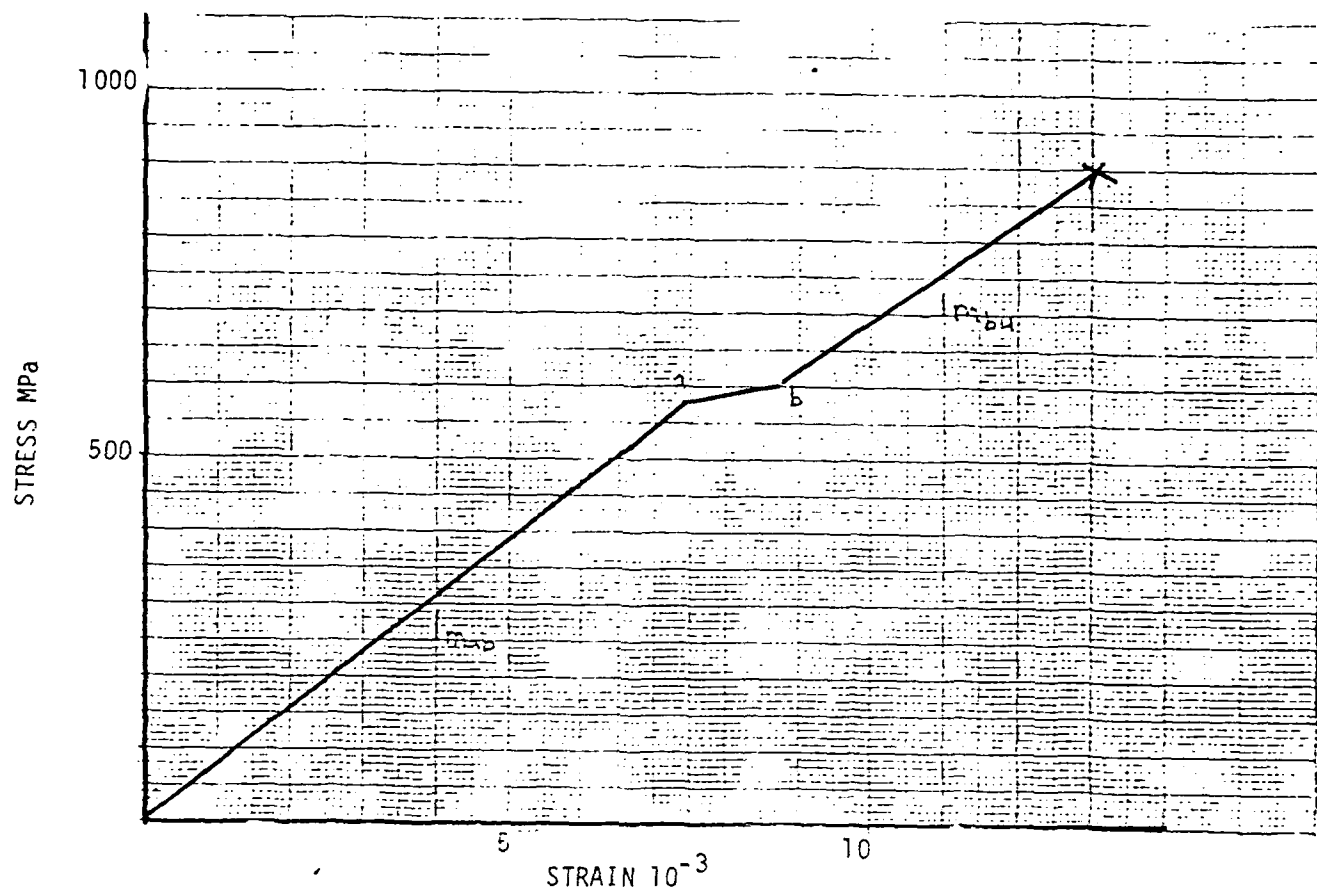
FIGURE 4 Typical Stress - Strain Curve for $(0_2 \pm 45)_s$
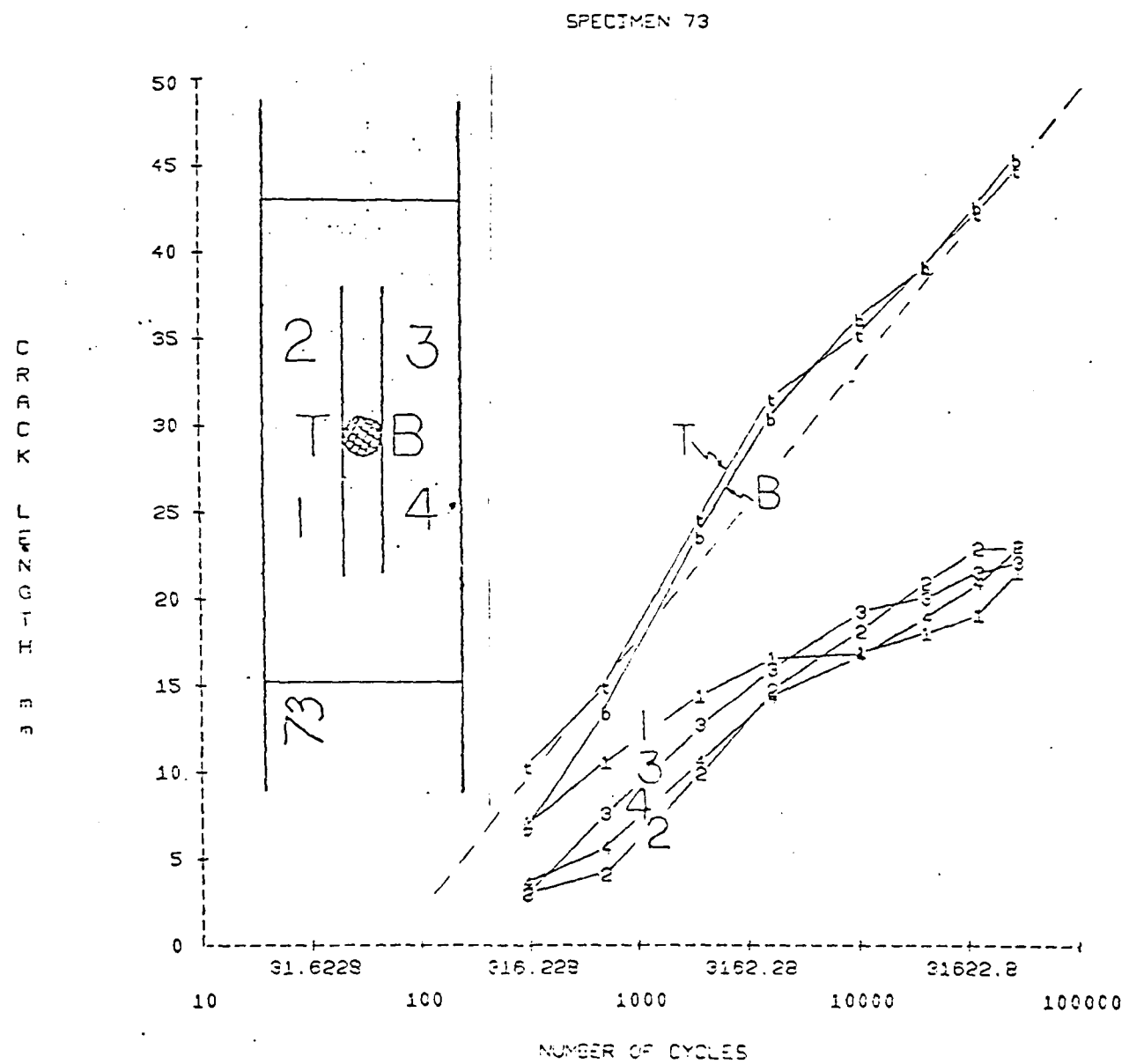
SPECIMEN 73

FIGURE 5:   Crack Length vs. Number of Cycles (#73)

TABLE I

TENSILE FRACTURE SPECIMENS

LAMINATE		HOLE DIAMETERS mm	TOTAL NO. OF SPECIMENS
$[0]_8$		--	--
$[0]_6$		--	10
$[0]_4$		--	5
$[0_2/\pm\theta]_s$	$\theta=0,15,30,45,75,90$	6.35	33
$[0/\pm\theta]_s$	$\theta=0,5,10,15$	0,3.18,6.35,9.53,12.70	190
$[\pm\theta/0]_s$	$\theta=0,5,10,15$	0,3.18,6.35,9.53,12.70	75

TABLE II

TENSION-TENSION CYCLICALLY LOADED SPECIMENS

$[0]_4$ with 3.2 mm holes

LOADING	NO. OF SPECIMENS
8% to 80% of splitting stress	17
7% to 70% of splitting stress	3
6% to 60% of splitting stress	4

splitting stress = 333 MPa

TABLE III

COMPRESSION-COMPRESSION CYCLICALLY LOADED SPECIMENS

Specimens with 12.7 mm Diam. Hole

LAMINATE		NO. OF SPECIMENS*
$[\pm45/0]_s$	CYCLED TO FAILURE	22
$[\pm45/0]_s$	CYCLED/RESIDUAL STRENGTH	26
$[0/\pm45]_s$	CYCLED TO FAILURE	3
$[0/\pm45]_s$	CYCLED/SECTIONED	1
$[\pm30/0]_s$	CYCLED/SECTIONED	2
$[0/\pm30]_s$	CYCLED/SECTION	2
$[0/\pm30]_s$	CYCLED/RESIDUAL STRENGTH	1

*Each specimen has two laminates.

TABLE IV

PARAMETERS FOR GROWTH OF SPLITS UNDER CYCLIC LOADS

CYCLIC LOAD LEVEL	NO. OF SPECIMENS	4	K	NO.
8% to 80%	17	15	28	65
7% to 70%	3	9	26	600
6% to 60%	4	5	20	3000

TABLE V

TESTING PROGRAM USED FOR INVESTIGATION

Specimen Type / Nominal Hole Size	$(0)_6$	$(0/\pm5)_s$	$(0/\pm10)_s$	$(0/\pm15)_s$
No Hole	U6-X	5B1-X	10B1-X	15B1-X
3.175 mm	U6-H2-X	5B1-H2-X	10B1-H2-X	15B1-H2-X
6.35 mm	U6-H4-X	5B1-H4-X	10B1-H4-X	15B1-H4-X
9.525 mm	U6-H6-X	5B1-H6-X	10B1-H6-X	15B1-H6-X
12.79 mm	U6-H8-X	5B1-H8-X	10B1-H8-X	15B1-H8-X

X = Specimen number, 1-10

10 specimens were made for each group (each box)

TABLE VI

TESTING PROGRAM USED FOR INVESTIGATION

Specimen Type / Nominal Hole Size	$(\pm 5/0)_s$	$(\pm 10/0)_s$	$(\pm 15/0)_s$
No Hole	5A1-X	10A1-X	15A1-X
3.175 mm	5A1-H2-X	10A1-H2-X	15A1-H2-X
6.35 mm	5A1-H4-X	10A1-H4-X	15A1-H4-X
9.525 mm	5A1-H6-X	10A1-H6-X	15A1-H6-X
12.70 mm	5A1-H8-X	10A1-H8-X	15A1-H8-X

X = Specimen number, 1-5

5 specimens were made for each group (each box)

TABLE VII

FAILURE STRESSES OF UNFLAWED $(0)_6$, $(0/\pm5)_s$, $(0/\pm10)_s$, AND $(0/\pm15)_s$ SPECIMENS

Specimen	σ_f (MPa)	Specimen	σ_f (MPa)
U6-1	1654.0	10B1-1	1090.6
U6-2	1644.8	10B1-2	1126.0
U6-3	1766.4	10B1-3	1142.8
U6-4	1516.2	10B1-4	1164.0
U6-5	1612.2	10B1-5	1160.9
U6-6	1754.8	10B1-6	1151.4
U6-7	1616.3	10B1-7	1142.7
U6-8	1421.4	10B1-8	1167.8
U6-9	1804.3	10B1-9	1172.8
U6-10	1818.8	10B1-10	1082.2
Average	1660.9 ± 128.4	Average	1140.1 ± 31.6
5B1-1	1285.5	15B1-1	1031.7
5B1-2	1264.2	15B1-2	1106.1
5B1-3	1255.1	15B1-3	1161.0
5B1-4	1179.2	15B1-4	1064.2
5B1-5	1271.8	15B1-5	1038.6
5B1-6	1221.9	15B1-6	1092.4
5B1-7	1299.6	15B1-7	977.3
5B1-8	1348.4	15B1-8	1035.0
5B1-9	1416.4	15B1-9	1068.2
5B1-10	1340.5	15B1-10	1010.2
Average	1288.3 ± 67.6	Average	1058.47 ± 52.3

σ_f = Gross Failure Stress

TABLE VIII

FAILURE STRESSES OF UNFLAWED
$(\pm 5/0)_s$, $(\pm 10/0)_s$, $(\pm 15/0)_s$ SPECIMENS

Specimen	σ_f (MPa)
5A1-1	1104
5A1-2	1232
5A1-3	999
5A1-4	1289
5A1-5	1048
Average	1134 ± 122
10A1 1	1046
10A1-2	985
10A1-3	961
10A1-4	987
10A1-	1103
Average	1016 ± 57
15A1-1	941
15A1-2	871
15A1-3	978
15A1-4	787
15A1-5	830
Average	891 ± 73

TABLE IX

FAILURE STRESSES OF $(0)_6$ SPECIMENS WITH HOLES

Specimen	σ_f(MPa)	Specimen	σ_f(MPa)
U6-H2-1	1661.8	U6-H6-1	1546.9
U6-H2-2	1576.5	U6-H6-2	1752.6
U6-H2-3	1605.6	U6-H6-3	1354.3
U6-H2-4	1650.7	U6-H6-4	1553.6
U6-H2-5	1670.7	U6-H6-5	1501.9
U6-H2-6	1635.7	U6-H6-6	1366.6
U6-H2-7	1551.8	U6-H6-7	1585.8
U6-H2-8	1699.6	U6-H6-8	1719.3
U6-H2-9	1440.3	U6-H6-9	1561.9
U6-H2-10	1652.1	U6-H6-10	1637.9
Average	1614.5	Average	1558.1
Std. Dev.	±75.7	Std. Dev.	±130.1
U6-H4-1	1777.3	U6-H8-1	1352.7
U6-H4-2	1446.7	U6-H8-2	1640.0
U6-H4-3	1465.6	U6-H8-3	1461.7
U6-H4-4	1446.9	U6-H8-4	1445.3
U6-H4-5	1395.6	U6-H7-5	1464.0
U6-H4-6	1313.0	U6-H8-6	1618.0
U6-H4.7	1723.9	U6-H8-7	1613.4
U6-H4-8	1561.9	U6-H8-8	1644.9
U6-H4-9	1483.3	U6-H8-9	1538.0
U6-H4-10	1513.1	U6-H8-10	1257.4
Average	1512.7	Average	1503.5
Std. Dev.	±142.4	Std. Dev.	±131.2

TABLE X

FAILURE STRESSES OF $(0/\pm5)_s$ SPECIMENS WITH HOLES

Specimen	σ_f(MPa)	Specimen	σ_f(MPA)
5B1-H2-1	1014.7	5B1-H6-1	762.4
5B1-H2-2	987.6	5B1-H6-2	725.6
5B1-H2-3	984.1	5B1-H6-3	747.9
5B1-H2-4	1015.9	5B1-H6-4	729.1
5B1-H2-5	1020.2	5B1-H6-5	727.2
5B1-H2-6	922.1	5B1-H6-6	805.3
5B1-H2-7	984.1	5B1-H6-7	698.9
5B1-H2-8	986.0	5B1-H6-8	763.0
5B1-H2-9	1049.0	5B1-H6-9	722.5
5B1-H2-10	921.1	5B1-H6-10	757.9
Average	988.5	Average	743.9
Std. Dev.	±40.9	Std. Dev.	±29.8
5B1-H4-1	917.7	5B1-H8-1	666.1
5B1-H4-2	811.1	5B1-H8-2	695.5
5B1-H4-3	811.5	5B1-H8-3	630.6
5B1-H4-4	824.7	5B1-H8-4	704.7
5B1-H4-5	1020.5	5B1-H8-5	712.4
5B1-H4-6	810.0	5B1-H8-6	719.0
5B1-H4-7	850.9	5B1-H8-7	639.9
5B1-H4-8	826.2	5B1-H8-8	666.8
5B1-H4-9	905.3	5B1-H8-9	735.4
5B1-H4-10	840.6	5B1-H8-10	700.2
Average	861.9	Average	687.1
Std. Dev.	±67.7	Std. Dev.	±34.7

TABLE XI

FAILURE STRESSES OF $(0/\pm10)_s$ SPECIMENS WITH HOLES

Specimen	σ_f(MPa)	Specimen	σ_f(MPa)
10B1-H2-1	696.6	10B1-H6-1	581.7
10B1-H2-2	828.7	10B1-H6-2	617.7
10B1-H2-3	831.2	10B1-H6-3	543.2
10B1-H2-4	707.6	10B1-H6-4	635.9
10B1-H2-5	722.6	10B1-H6-5	580.0
10B1-H2-6	762.3	10B1-H6-6	595.3
10B1-H2-7	753.8	10B1-H6-7	526.9
10B1-H2-8	787.9	10B1-H6-8	559.6
10B1-H2-9	885.2	10B1-H6-9	630.8
10B1-H2-10	763.9	10B1-H6-10	511.3
Average	774.0	Average	578.2
Std. Dev.	±60.1	Std. Dev.	±43.0
10B1-H4-1	739.5	10B1-H8-1	519.4
10B1-H4-2	650.7	10B1-H8-2	574.4
10B1-H4-3	703.8	10B1-H8-3	493.7
10B1-H4-4	669.5	10B1-H8-4	497.9
10B1-H4-5	707.7	10B1-H8-5	592.6
10B1-H4-6	670.8	10B1-H8-6	579.8
10B1-H4-7	607.9	10B1-H8-7	574.1
10B1-H4-8	803.8	10B1-H8-8	466.3
10B1-H4-9	635.3	10B1-H8-9	510.7
10B1-H4-10	697.6	10B1-H8-10	593.3
Average	688.7	Average	540.2
Std. Dev.	±55.8	Std. Dev.	±47.3

TABLE XII

FAILURE STRESSES OF $(0/\pm15)_s$ SPECIMENS WITH HOLES

Specimen	σ_f(MPa)	Specimen	σ_f(MPa)
15B1-H2-1	613.00	15B1-H6-1	414.70
15B1-H2-2	600.20	15B1-H6-2	453.80
15B1-H2-3	681.90	15B1-H6-3	474.60
15B1-H2-4	544.60	15B1-H6-4	404.20
15B1-H2-5	635.10	15B1-H6-5	440.30
15B1-H2-6	650.00	15B1-H6-6	467.80
15B1-H2-7	670.80	15B1-H6-7	489.80
15B1-H2-8	711.50	15B1-H6-8	451.90
15B1-H2-9	702.30	15B1-H6-9	391.10
15B1-H2-10	646.80	15B1-H6-10	488.70
Average	645.52	Average	447.69
Std. Dev.	±50.49	Std. Dev.	±34.76
15B1-H4-1	589.60	15B1-H8-1	401.00
15B1-H4-2	483.30	15B1-H8-2	397.40
15B1-H4-3	604.70	15B1-H8-3	368.30
15B1-H4-4	540.00	15B1-H8-4	362.70
15B1-H4-5	511.60	15B1-H8-5	428.20
15B1-H4-6	539.00	15B1-H8-6	382.90
15B1-H4-7	503.90	15B1-H8-7	353.20
15B1-H4-8	481.20	15B1-H8-8	365.00
15B1-H4-9	539.10	15B1-H8-9	403.00
15B1-H4-10	535.50	15B1-H8-10	398.80
Average	532.79	Average	386.05
Std. Dev.	±40.73	Std. Dev.	±23.50

TABLE XIII

FAILURE STRESSES OF $(\pm 5/0)_s$ SPECIMENS WITH HOLES

Specimen	σ_f(MPa)
5A1-H2-1	898
5A1-H2-2	915
5A1-H2-3	970
5A1-H2-4	927
5A1-H2-5	998
Average	942 ± 41
5A1-H4-1	936
5A1-H4-2	849
5A1-H4-3	774
5A1-H4-4	751
5A1-H4-5	870
Average	836 ± 75
5A1-H6-1	843
5A1-H6-2	830
5A1-H6-3	830
5A1-H6-4	841
5A1-H6-5	665
Average	802 ± 77
5A1-H8-1	664
5A1-H8-2	745
5A1-H8-3	713
5A1-H8-4	671
5A1-H8-5	681
Average	695 ± 34

TABLE XIV

FAILURE STRESSES OF $(\pm 10/0)_s$ SPECIMENS WITH HOLES

Specimen	σ_f
10A1-H2-1	794
10A1-H2-2	880
10A1-H2-3	790
10A1-H2-4	937
10A1-H2-5	857
Average	852 ± 62
10A1-H4-1	769
10A1-H4-2	624
10A1-H4-3	655
10A1-H4-4	740
10A1-H4-5	727
Average	703 ± 61
10A1-H6-1	427
10A1-H6-2	534
10A1-H6-3	491
10A1-H6-4	608
10A1-H6-5	593
Average	525 ± 69
10A1-H8-1	567
10A1-H8-2	617
10A1-H8-3	491
10A1-H8-4	458
10A1-H8-5	478
Average	522 ± 67

TABLE XV

FAILURE STRESSES OF $(\pm 15/0)_s$ SPECIMENS WITH HOLES

Specimen	σ_f(MPa)
15A1-H2-1	608
15A1-H2-2	646
15A1-H2-3	800
15A1-H2-4	558
15A1-H2-5	670
Average	656 ± 90
15A1-H4-1	412
15A1-H4-2	682
15A1-H4-3	516
15A1-H4-4	600
15A1-H4-5	440
Average	530 ± 112
15A1-H6-1	482
15A1-H6-2	506
15A1-H6-3	540
15A1-H6-4	527
15A1-H6-5	509
Average	512 ± 22
15A1-H8-1	431
15A1-H8-2	363
15A1-H8-3	511
15A1-H8-4	329
15A1-H8-5	432
Average	413 ± 70

TABLE XVI

H_c, COMPOSITE TOUGHNESS AND m, SINGULARITY

LAMINATE	m**	H_c*
$[0/\pm 5]_s$	.22	1300
$[\pm 5/0]_s$	.15	1140
$[0/\pm 10]_s$	.24	1060
$[\pm 10/0]_s$	.32	1260
$[0/\pm 15]_s$	.34	990
$[\pm 15/0]_s$	.26	900

*Dimensions of H_c are MPa $(mm)^{-m}$

**Failure stresses were modified by a finite width correction.

COUPLING ACTIVITIES

The Principal Investigator, Prof. James W. Mar is a member of

a) the USAF Scientific Advisory Board,

b) NASA Space Systems Technology Advisory Committee,

c) the National Materials Advisory Board of the NRC Commission on Sociotechnical Systems,

d) chairman of the F-18 Structural Integrity Panel for the Assistant Secretary of the Navy for Research, Engineering and Systems, and

e) in December of 1980 it was announced that Prof. Mar would also be the new department head effective 1 July 1981 in the Department of Aeronautics and Astronautics at M.I.T.

PUBLICATIONS

1. Fanucci, Jerome, "Damage Initiation and Propagation During Compressive Fatigue of Flawed Graphite/Epoxy Composites," Ph.D. Dissertation, Dept. of Aeronautics and Astronautics, M.I.T., February 1980.

2. Lesieutre, George, "Failure Modes of $[0_2+0]_s$ Graphite/Epoxy Laminates," M.I.T. Technology Laboratory for Advanced Composites (TELAC) Report, March 1980.

3. Heimann, Thomas, "Predicting the Contours of Asymmetric Graphite/Epoxy Laminates," M.I.T., Dept. of Aeronautics and Astronautics Undergraduate Course (16.62) Report, May 1980.

4. Lesieutre, George, "Crack Growth in 4-Ply Unidirectional Graphite/Epoxy Laminates Under Cyclic Loading," M.I.T., Dept. of Aeronautics and Astronautics Undergraduate Course (16.62) Report, May 1980.

5. Lussier, David, "Predicting the Contours of Asymmetric Graphite/Epoxy Laminates," M.I.T., Dept. of Aeronautics and Astronautics Undergraduate Course (16.62) Report, May 1980.

6. Mar, James; Graves, Michael; and Maass, David, "The Effects of Compression-Compression Fatigue on Balanced Graphite/Epoxy," presented at the AIAA/ASME/ASCE/AHS 21st Structures, Structural Dynamics and Materials Conference, 12-14 May 1980, Seattle, Washington.

7. Garcia, Jose, "Static Tensile Behavior of $(0)_6$, $(0/\pm5)_s$, $(0/\pm10)_s$, and $(0/\pm15)_s$ Graphite/Epoxy Laminates with Holes," S.M. Dissertation, Dept. of Aeronautics and Astronautics, M.I.T., June 1980.

8. Lee, Mark, "Fatigue in Graphite/Epoxy Bolted Joints," S.M. Dissertation, Dept. of Mechanical Engineering, M.I.T., June 1980.

9. Garcia, Jose, "$(\pm\theta/0)$, θ = 5, 10, 15," M.I.T. Technology Laboratory for Advanced Composites (TELAC) Report, August 1980.

10. Mar, James; and Lagace, Paul, "Tensile Fracture of Graphite/Epoxy Laminates with Holes," presented at the 3rd ICCM Conference, Paris, France, 25-30 August 1980.

11. Hollowell, Stephen, "Aeroelastic Flutter and Divergence of Graphite/Epoxy Cantilevered Plates with Bending-Torsion Stiffness Coupling," S.M. Dissertation, Dept. of Aeronautics and Astronautics, M.I.T., January 1981.

APPENDIX A

DAMAGE INITIATION AND PROPAGATION DURING COMPRESSIVE

FATIGUE OF FLAWED GRAPHITE/EPOXY COMPOSITES

TABLE OF CONTENTS

Chapter I

INTRODUCTION

Within the past decade graphite/epoxy composite material
has matured as a viable alternative to metals for use in
high technology structures. Its comparatively low density
combined with high strength and stiffness make it particu-
larly suited for aerospace applications, where weight reduc-
tion is always a primary concern. Graphite/epoxy's excel-
lent performance as a structural material stems from its
orthotropic material properties. In a strength designed
composite component, the fibers of individual plys can
ideally be oriented to produce a laminate with no excess
strength in any direction. An equivalent metallic component,
sized to carry a maximum load in the direction of the prin-
cipal stress, is usually overdesigned when viewed from any
other direction. The cost of this unavoidable overdesign, a
direct result of metal's isotropic properties, is increased
structural weight.

Another benefit resulting from graphite/epoxy's ortho-
tropy is the possibility 'of creating specialized laminate
properties by careful selection of ply stacking sequence.
Aeroelastically tailored, bending-twisting coupled forward
swept wings and near zero coefficient of thermal expansion

space structures are two of the more sophisticated graphite/epoxy applications currently under study. The success of each of these designs depends upon the employment of unusual laminate properties which can not be economically duplicated using metals technology.

Several aircraft companies have demonstrated substantial manufacturing cost reductions when replacing a metal component with a composite piece. These savings are a result of graphite/epoxy's molded fabrication. Often up to 90% of a billet or forging is turned to scrap chips during the machining of a complicated shape from a metal block. In comparison, waste of graphite/epoxy has been shown to be in the 10 to 20 percent range. Metal designs that for manufacturing reasons must consist of several parts fastened by rows of rivets can often be produced as a single composite component. The reduced inventory and simplified assembly resulting from the use of composites tends to lower manufacturing costs. As an additional benefit, the smaller number of part interfaces and fasteners improves structural performance by lowering the number of stress concentrations.

Because graphite/epoxy is a relatively new material, insufficient amounts of statistically significant data and few experimentally proven analytical methods exist. Without these, the aggressive exploitation of its properties is impossible. Commercial airframe manufacturers have been

hesitant to make a major commitment to the material before a more thorough understanding of its long term behavioral characteristics is obtained. In the interim they have limited its use to easily removable, stiffness designed components such as control surfaces, landing gear doors and fairings. One of the major thrusts in composite research, aimed at providing information of the type required for structural life predictions, has been the study of graphite/epoxy's fatigue properties.

Early fatigue work focused on determining the material's response to cyclic tensile stresses. Awerbuch and Hahn's (1) examination of the behavior of unidirectional coupon specimens is typical of these tensile fatigue investigations. In addition to the usual measurement of life to failure and residual static strength over a range of peak stress levels, this study included the effect of a proof load on the fatigue life distribution. A proof load is a large static load applied prior to cycling. It was hoped that this load would indicate some relationship between the static strength distribution of virgin coupons and their fatigue life by eliminating specimens of low static strength. While their program was not able to conclusively show that the strength and life distributions of a population of graphite/epoxy specimens are related, it did serve as an important source of experimental data for statistical fatigue life prediction methods.

Many of these life prediction methods are based on the strength-life equal rank assumption first introduced by Hahn and Kim (15). This hypothesis states that in a group of specimens, the one with the greatest static strength will also have the longest fatigue life. The lowest strength specimen will be the first to fail under fatigue loading. Static strength and fatigue life of any particular specimen will occupy the same position in the two ordered sets of strength and life data. Chou and Wang (5) compiled data from various tensile fatigue experiments and compared several strength degradation and failure models based on the equal rank assumption. None were found to satisfactorily describe every set of experimental data.

One unexpected result of fatigue tests using laminates with circular holes and other flaws was the discovery that static strength often substantially increases during fatigue cycling. Ramani and Williams (28), for example, present data displaying up to 40% increases in residual static strength after 5 million tension-tension cycles. Reifsnider, Stinchcomb, and O'Brien (31) explain this unusual behavior as the simultaneous interaction between a wear-in and wear-out process. Wear-in occurs locally as the multiple damage modes available to a composite laminate erase the stress concentration at the discontinuity. Wear-out consists of a general degradation of the entire laminate by repeated loading. The sum of these two processes first

results in a net increase in strength due to wear-in and later a decrease as wear-out becomes dominant.

Of particular importance to the future employment of graphite/epoxy are the studies showing that specimens subjected to cyclic tensile loads often display fatigue limit type behavior when tested at peak loads below approximately 60% of the laminate's static ultimate strength. The fatigue limit is defined as the load below which a structure will survive an infinite (or at least extremely large) number of cycles. Grimes (11), in a paper discussing the significance of these findings, writes, "This behavior is quite different from metals, and better. Graphite/epoxy endurance limits are not only truer in a physical sense, but they are higher in magnitude than those artificially defined values for metals. Structures with nearly unlimited lifetimes appear possible, at least on paper, if the working stresses are kept below the initial fatigue endurance limit stress level."

The inclusion of compressive loads in the fatigue spectrum has been shown to significantly reduce life to specimen failure. In an often quoted report, Ryder and Walker (37) conclusively demonstrate this point by presenting results of tension-tension, tension-compression, and compression-compression fatigue of two different laminates. The slope of both the tension-compression and compression-compression S-N curves is much steeper than the tension-tension curve, with

the load reversal case being the most critical. This indi-
cates that the introduction of compressive cyclic loads can
greatly shorten fatigue life. Rosenfeld and Huang (34) pos-
tulate that matrix strength is reduced to a point where
fibers can buckle under a compressive load. This tends to
produce more damage per cycle than an equivalent tensile
load, and accounts for the reduction in life compared to
tensile fatigue.

The importance of compressive loads in graphite/epoxy
fatigue is directly opposed to previous experience with
metals. This behavioral difference can be explained by exa-
mining the damage modes available to both. In metal fati-
gue, crack growth perpendicular to the load direction is the
only important form of damage. A tensile load, which pro-
duces a theoretically infinite stress concentration at a
sharp notch, causes extension by separating crack surfaces.
Compressive loads force these opposing surfaces together,
and therefore have little tendency to extend metallic
cracks. Due to the nonhomogeneous nature of a composite
laminate, many other damage modes besides crack extension
can exist. Fiber breaks, delamination, matrix cracking and
fiber/matrix debonding are all important damage modes, uni-
que to composites, which may be induced by static or cyclic
loading. When compressive loads are applied, damage to sur-
face plys locally separated from the bulk of a specimen by
delamination can often be accelerated by buckling of these
unsupported regions.

A major source of aggravation to the many composite lami-
nate damage modes is the three-dimensional nature of the
stress field existing near free edges and cutouts. Interla-
minar shear along with out-of-plane shear and normal stress
develop to satisfy the stress free boundary condition at
unloaded edge surfaces. These stresses, often comparable
in magnitude to the average far field applied axial stress,
have been shown to exist within a narrow edge region on the
order of one laminate thick. Classical laminate theory
ignores these out-of-plane stress components, and therefore
is unlikely to accurately predict the stress distribution at
precisely the location where fatigue is most likely to begin
- at a free edge or other flaw in the laminate. When one
considers the inherent property scatter, variety of damage
modes and complex stress distribution in even a simple gra-
phite/epoxy coupon specimen, it is understandable why past
analytical, empirical and experimental attempts at fatigue
life prediction have met with limited success.

Recent work by Graves (10) suggested a different approach
to the investigation of composite fatigue. Results of this
compressive fatigue experiment, conducted using flawed sand-
wich beam specimens in four point beam bending, indicated
that pre-failure damage propagation behavior may be more
consistently predictable than cycles to final failure. The
data showed that even after developing extensive areas of
visible damage, specimens could survive a significant number

of additional fatigue cycles before failure. While the behavior of composite laminates after damage has initiated is extremely important for modern damage tolerant aircraft structural designs, very little of this type of information is available in the current literature.

The research described in this report was conducted to more rigorously investigate the damage initiation and propagation behavior of graphite/epoxy laminates with circular holes during compressive fatigue. Eighty-nine axially loaded, aluminum honeycomb sandwich specimens with graphite/epoxy face sheets of four diffent laminates, $(\pm45/0)s$, $(0/\pm45)s$, $(\pm30/0)s$ and $(0/\pm30)s$ were compressively cycled with a minimum to maximum load ratio of R=10. Fatigue damage initiation and propagation were monitored on both graphite/epoxy faces of each specimen using Moire interferometry, a method of optically producing surface contour lines. These patterns were photographically recorded at intervals for later analysis. Life, residual strength, cycles to damage initiation and damage growth data are reported. Damage initiation site and mode are compared with the analytically predicted three dimensional stress field at the edge of the hole.

Chapter II

EXPERIMENTAL METHOD

2.1   SPECIMEN SELECTION

One of the major difficulties of compressive testing is
the introduction of high compressive loads into a specimen
without inducing buckling.   Three test method and specimen
configuration combinations,   designed to   minimize buckling
problems,   were considered for use   in this program- (1)
externally supported coupons, (2)   sandwich beam in four
point bending, and (3) axially loaded sandwich columns.

A preliminary investigation using full and partial exter-
nal coupon supports modeled after those described by Ryder
and Walker of Lockheed (37) was conducted. Resulting failure
mode and location seemed to be highly dependent on support
configuration, probably due to the thinness (less than 1mm)
of the six ply laminates.   The further complication of sup-
port compatiblity with nondestructive inspection (NDI) meth-
ods led to the rejection of supported coupon specimens. Four
point bending sandwich beams of the type employed by Graves
(10) were also rejected. It was felt that the concave curva-
ture of the compressive face would accelerate the expected
delamination failure mode by increasing the tendency of the
outer plys to buckle away from the laminate after initial
damage.

Axially loaded sandwich columns were selected for use in this program for several reasons. The outer surfaces of the specimen were free of supports and thus accessable to NDI, while general buckling of the 2.5mm thick sandwich was negligible at loads up to the specimen's static failure load (See Section 4.1). Both graphite/epoxy faces simultaneously experienced the same load history; two sets of initiation and propagation data were therefore generated with each test run.

2.2   SANDWICH COLUMN FABRICATION

A total of one hundred sandwich beam specimens, some of which were used in the development of test methods and will not be further mentioned, were fabricated. Forty-four 30.5cm. square, six-ply laminates of four different orientations were constructed from 30.5cm. wide AS1/5208-6 graphite/epoxy tape. Laminates were cured in batches of two to six using the standardized autoclave/vacuum bag/tooling procedures and cycles developed at MIT (90). Cured laminates were cut into five 5x30cm. coupons with a water cooled diamond wheel mounted on an automatically fed milling machine. The two resulting 2.5cm. wide edge strips were discarded. The centrally located 1.25cm. diameter hole in each coupon was made using a water cooled diamond drill. Punch through damage to the bottom ply of the coupons during the hole drilling operation was minimized by backing up the piece being drilled with graphite/epoxy scrap.

The core of the sandwich specimens was composed of three separate pieces of 6cm. wide American Cyanamid Aluminum Honeycomb. A central 17.5cm. long 72kg/m3 (4.5lb/ft3) test section was bounded by two 6.25cm. long, 354kg/m3 (22.1lb/ft3) pieces. The heavier density core was required near the specimen's ends to withstand the 2.07 to 3.45 MPa (300 to 500 psi) normal load applied by the testing machine's hydraulic grips.

Actual assembly of the specimens was carried out in two separate operations. Graphite/epoxy face sheets were bonded to the three core pieces, which had first been cleaned in MEK, using American Cyanamid FM-123 film adhesive. Another American Cyanimid adhesive, FM-37-2, was used to bond the individual core pieces during the same operation. Four 7.5x6.25cm. $(0_2/90_2)$s fiberglass loading tabs were later bonded, with a 1.25cm. overlap of the core splice, to the graphite/epoxy face sheets using FM-123 (see Figure 1). All bonding operations were conducted using a hot press.

2.3 NONDESTRUCTIVE INSPECTION BY MOIRE INTERFEROMETRY

Choice of a suitable nondestructive inspection method was of fundamental importance to the successful completion of this experimental investigation. Required NDI characteristics included in situ application, long term stability, repeatability, low cost, passive operation and sensitivity to expected damage modes. A survey of methods indicated that Moire interferometry best met the above criteria.

Moire interferometry uses the interference pattern formed by the relative motion of two sets of fine parallel lines to visually provide a map of surface displacement. Although not actually used for this experiment, the physics of this method can most easily be explained by examining the more commonly employed case of in-plane interferometry for measurement of in-plane strains. Typically, a grill of evenly spaced, parallel black lines and equal width clear spaces is in some manner fixed to the undeformed surface to be examined. This grill will deform with the specimen surface (Figure 2a). An identical reference grill applied to a glass plate is then placed near the prepared specimen. No interference pattern will develop if the reference grill is arranged to have each of its lines lie directly on top of a specimen line (Figure 2b). When the rigid reference glass is moved the width of one line in a direction perpendicular to the lines, each black line of the reference grill will fall directly above a clear space on the specimen, and vice-versa. The result is completely destructive interference, or a uniformly dark pattern (Figure 2c). By stretching the specimen, however, the attached grill can be made to contain fewer lines/unit length than the reference grill. This creates a gradual change from a totally dark to totally clear pattern. Each of the resulting bright or dark lines is termed a fringe. The distance between two equal intensity fringes is related to the known grill line spacing; relative

displacement of points on the surface can therefore be cal-
culated by simply counting fringes between points (Figure
2d).

Delamination was the primary damage mode exhibited by the
composite specimens in this experiment. When the compressive
force applied during each loading cycle reached some criti-
cal value, delaminated areas developed during fatigue
cycling would buckle. A modification of the in-plane mea-
surement technique described in the preceding paragraph was
employed to produce a visual indication of these small out-
of-plane surface deformations (Figure 3). To measure out-
of-plane displacements with this technique,the reference
grill is positioned close to and parallel with the initially
planar column face to be inspected. A collimated light
source, placed at an angle of between 40 and 70 degrees with
the surface, is used to illuminate the specimen. Since the
grill is located between the light source and specimen, sha-
dows of each of its lines are cast on the sandwich column.
For a reasonably parallel beam of light, these shadow lines
reproduce the reference grill pattern and take the place of
the physically applied grill used for in-plane measurements.

When a portion of the surface undergoes out-of-plane dis-
placement due to local buckling, the shadow lines in that
region are distorted. This results in the formation of
interference patterns by a process similar to the one previ-

ously described. It can be shown that the resulting pat-
terns actually are surface contour lines. The difference in
height between two successive fringes can be calculated
using:

$$\Delta z = 1/n \tan\theta$$

where Δz is change in height between two successive fringes,
n is the density of the grill in lines per unit length and θ
is the angle between the light beam and the specimen's sur-
face perpendicular.

In a setup repeated on both sides of the column, a 100
line/inch grill was mounted on a six degree of freedom
holder and positioned less than 0.25cm. from the specimen
(Figure 4). Photoelastic, Inc.'s Tens-Lac Type U-10-A Brit-
tle Lacquer Undercoating, a silver colored spray, was used
to paint the sandwich column faces for increased Moire pat-
tern contrast. Thirty-five millimeter slide projectors
angled 50 degrees from the specimen served as light sources.
Zoom lenses with knife edge slits mounted in front of their
outer elements provided adequately collimated beams (Figure
5). From equation 1, the resulting Δz between adjoining
fringes can be shown to be 0.021cm. Since it was usually
possible to discern 1/4 fringe intensity changes, out-of-
plane motion of approximately 0.005cm. could normally be
sensed.

One difficulty arising early in the test program was the formation of an interference pattern between the reference grill lines and the peel-ply textured surface of the graphite/epoxy. It was found that the visibility of this secondary pattern could be greatly reduced by slightly rotating the reference grill such that its originally vertical lines were tilted approximately 10 degrees. This action produced no visible change in the observed damage patterns.

2.4 TEST PROCEDURE

All testing was conducted on a 100,000lb Material Test Systems Model 810 testing machine operated in the 10,000lb range. To prevent slippage, specimens were held in MTS hydraulic grips adjusted to apply a 2.07 to 3.45 MPa (300 to 500 psi) normal load to the fiberglass loading tabs. The net section static compressive strength of all four laminate types was established using axially loaded columns identical in design to the fatigue specimens. Two back to back 6.35 mm BLH Type FAE-25-12-S3 strain gauges, one on each column face of most static specimens (Figure 1), were monitored during loading using BLH 1000 digital strain indicators. Besides allowing the calculation of laminate modulus of elasticity, the linearity of the strain data confirmed that no generalized specimen buckling occurred before static failure (Figure 6). Stroke controlled tests were run at a strain rate of 0.0006 per minute. When possible, load was

released after failure of just one graphite/epoxy column face.

Fatigue tests of the axially loaded column specimens were conducted on the same MTS testing machine. Test loads were chosen to span the range between static failure and the fatigue limit with a fairly uniform distribution of data points. Monitoring of the maximum and minimum compressive loads while cyling at 20 Hz and R=10 revealed some difficulty in following the commanded sinusoidal program. Slight reduction of the cyclic frequency eliminated this system resonsance problem; thus, the majority of fatigue testing was performed at 19 Hz. Other workers (32) have reported that high cycling rates during a fatigue test can induce temperature rises that alter matrix properties. 19 Hz. was chosen as a compromise between the minimization of this temperature effect and the reduction of test time. In some tests, frequency was gradually increased from 0.1Hz to 19Hz during the first 400 cycles to reduce the likelihood of startup failures. - This practice proved to be unnecessary and was discontinued early in the program. Cycling was periodically halted for between 2 and 5 seconds to permit Moire pattern photographs to be taken. A static force of slightly more than half the maximum compressive load was maintained during this period. The increment between successive pictures was varied to produce approximately even spacing on a log(cycles) plot. Maximum exposure rate followed the schedule below:

RANGE(CYCLES)	CYCLES BETWEEN EXPOSURES	MAXIMUM NUMBER OF EXPOSURES	TIME BETWEEN EXPOSURES(MINUTES) AT 19 HZ
0 - 1000	200	6	0.175
1250 - 4000	250	12	0.219
4500 - 10000	500	12	0.439
11000 - 20000	1000	10	0.877
22500 - 45000	2500	10	2.193
50000 - 120000	5000	15	4.386
130000 - 300000	10000	18	8.772
320000 - 600000	20000	15	17.544

Many of the low cycle pictures were skipped during low stress level tests when experience indicated damage would not initiate early in the specimen's life.

If fracture did not occur by 600,000 cycles, standard procedure was to immediately conduct a residual strength test by gradually increasing compressive load until static failure was induced. Fatigue loading of a few specimens was extended, with two specimens tested to one million cycles. Ten specimens were removed from the testing machine before final failure. Microscopic examination of cross sections taken near the edge of the hole allowed comparison of Moire patterns with actual laminate damage.

Pseudo-random specimen and test condition selection was employed to prevent data biasing. Whenever possible, specimens manufactured from laminates cured in the same autoclave batch were distributed over a range of load conditions. The test program's history can be reconstructed from the chronologically sequenced run numbers listed in Tables 1 and 2.

2.5 PHOTOGRAPHIC TECHNIQUE

The intensity difference between light and dark fringes of Moire patterns is normally low. Because a major objective of the investigation was the producion of a photographic record of damage initiation and propagation, care was taken to increase the pattern contrast whenever possible. The selection of a 100 line/inch grill was driven mainly by this concern. Measurement sensitivity could be increased by employing a grill of higher line density, but only at the expense of pattern visibility.

Moire pattern photographs were taken with two 35mm cameras; a motor driven Nikon F2A equiped with a Nikon 100mm Micro lens was mounted behind the specimen and an Olympus OM-1 with a Vivitar 90mm Macro lens in the front. Kodak PLUS-X black and white film was used throughout the experiment. By intentionally underexposing by 2 f/stops and doubling normal development time, contrast on the negative was increased to the point where pattern visibility was not a problem during measurement and printing of the images.

Chapter III

ANALYSIS

3.1   THREE DIMENSIONAL STRESS FIELD PREDICTION

Experimental   evidence   has   indicated   that   stacking
sequence does affect both the fatigue life and pre-failure
behavior of G/E laminates.   In a more complete analysis of a
laminate's stress field, Pipes and Pagano (86) used a finite
difference   technique   to   show   that   large   interlaminar
stresses can be developed in a narrow region near the
straight free edge of a coupon specimen.   Furthermore, it
was found that reversing the stacking sequence of those sim-
ple laminates changed the orientation of the out-of-plane
normal stress from tension to compression. Since the lami-
nate found to have a tensile interlaminar stress corresponds
with stacking sequence experimentally shown to have a
shorter fatigue life (22), it has been hypothesized that
tensile interlaminar normal forces shorten life by acceler-
ating propagation of fatigue induced delaminations.

A special laminated plate traction-free edge finite ele-
ment was developed by Harris (62) for analysis of more com-
plicated geometries than straight free edges.   While this
element requires the use of far fewer degrees of freedom
than would normally be necessry if non-specialized elements

were employed to calculate the laminate's three dimensional stress field, the amount of computer storage and time needed to analyze even relatively thin laminates is still very large. Also, the oscillatory nature of some of its predicted stress components reduces confidence in the ability of its forth order polynomial approximation of element stress to accurately predict behavior.

A more elegant method for prediction of the three dimensional stress field in composite laminates is currently under development by Bar-Yoseph (52). By applying the well established fluid dynamics technique of matched asymptotic expansion to the equilibrium equations, the problem was separated into an inner region decribed by simple laminate theory and an outer region whose mathematical description included all six stress components. Asymptotic series descriptions of the stress field in powers of the small parameter, h/l, the ply thickness nondimensionalized by some characteristic length, were substituted into the two equation sets. The stress free edge boundary conditions were satisfied exactly by imposing the condition that the sum of the inner and outer solutions of certain components must be zero at the free edge. Other charateristics of the series were determined from matching of equal order terms, using the fact that at some intermediate region the solutions must agree. With only terms of the first order in h/l retained for this preliminary application of his analysis, Bar-Yoseph

developed assumed expressions for the stress components of the boundary layer solution of symmetric laminates in terms of just four exponentially decaying position dependent constants per laminate ply. Solution of the 3-D stress distribution around a hole was therefore reduced to determining just 4n-2 constants, where n is half the number of plys in a symmetric laminate. Note that two constants are determined from symmetry conditions. Substitution of these expressions into a complementary energy variational formulation resulted in a set of fourth order differential equations. By casting these in the form of an eigenvalue problem, standard solution techniques could be used to determine the unknown constants in the stress functions. With these constants known, the calculation of a stress at any point in the laminate simply requires substitution of the coordinates into the appropriate equation.

Chapter IV

DATA REDUCTION

4.1 APPLIED STRESS DETERMINATION

The axially loaded sandwich column specimens used in this test program did not buckle at loads below the ultimate compressive strength of the graphite/epoxy laminates. Therefore, the strain experienced by each of the two face sheets should be equal. If the axial modulus of each laminate is also assumed to be equal then the applied stress can be estimated by simply dividing the applied load by the total of the two face sheet's cross sectional areas. With the exception of the far field stress used in laminate modulus calculations, all stresses in this report are average net section stresses based on the cross sectional area at the hole.

The graphite/epoxy manufacturer's nominal thickness of 0.8001mm for a 6 ply laminate was used for all area determinations. Actual measured laminate thickness averaged about 10% higher. Microscopic examination of laminates revealed the source of this discrepancy to be a thin textured layer of epoxy on both outer laminate surfaces. These layers formed when excess resin material hardened in the finely woven fiberglass cloth peel-ply which surrounded the graphite/epoxy during curing.

When the peel-ply was removed, an imprint of the fabric's texture was left on the laminate's surface. The total top and bottom thickness of these resin layers almost exactly corresponds to the difference between measured and nominal thickness. Because the resin rich surface layers are essentially unloaded, it was decided to ignore their contribution to total laminate thickness for all stress calculations in this report.

4.2   LAMINATE MODULUS DETERMINATION

Ten strain gauged specimens were statically tested to determine the longitudinal modulus of the four laminate types used in this program. Strains, recorded every 200lbs. during loading, were plotted versus the far field stress. Modulus was calculated by finding the slope of the best line through this data using linear regression analysis. The correlation coefficient, an indication of the linearity of the 30 to 40 data points used for modulus calculations, was also determined for each laminate (Table 1).

4.3   DAMAGE INITIATION MEASUREMENTS

Determination of the number of cycles of fatigue loading endured by the graphite/epoxy column faces before the onset of detectable damage was a primary objective of this test program. Negatives of the Moire pattern photographs, taken at intervals during fatigue testing, were compared with the

0 cycle photograph under 10x magnification. By starting from a point where damage was clearly visible and tracing backwards through the negatives, it was possible to locate the earliest frame where damage could be seen. The number of load cycles corresponding to this frame was recorded as the laminate's life to first detectable damage. The circumferential location of the damage initiation site was found by projection of the frame containing first damage onto a piece of polar graph paper. Positive angles were defined as being counterclockwise from the load direction, with the top of the specimen as tested defined as zero.

Choice of the negative containing the onset of fatigue damage was not always obvious, especially in laminates where it occurred after several hundred thousand load cycles. In some cases where damage developed very slowly, an uncertainty in cycles to initiation of one or two negatives was possible. This corresponds to a possible error of ± 400 to 40,000 cycles, depending on when in the laminates life the damage initiated. This error is relatively small when compared to the order of magnitude scatter typical of fatigue life data.

4.4 DAMAGE AREA MEASUREMENT

In order to quantify the damage propagation behavior in graphite/epoxy laminates after initiation, the surface area bounded by the outermost Moire fringe lines was measured for

a succession of individual frames. Every laminate that demonstrated significant growth prior to failure or test termination was measured. Selected negatives were projected from the rear onto a large ground glass table top; the resulting image was enlarged to approximately ten times life size to facilitate measurement. A planimeter was then used to mechanically calculate the area contained inside the Moire pattern. By also measuring the area of the projected hole, a simple ratio could be used to determine the actual damage area existing on the specimen.

Chapter V

RESULTS

5.1 STATIC TEST DATA

Seventeen specimens, all containing 1.25 cm. diameter holes, were statically loaded to failure in axial compression. Laminate moduli and ultimate net section compressive strengths determined from these tests are listed in Tables 1a and 1b. Of particular note are the high values of R, the linear correlation coefficient, found for those static tests conducted using strain gauges. Since R=1 implies perfectly linear data, these numbers indicate that generalized buckling of the axially loaded column specimens did not occur prior to compressive failure (Figure 5). Table 1b shows an unusual result of the ultimate strength measurements. Although intuition would indicate otherwise, specimens with the angle plys at 45 degrees were found to fail at higher average compressive loads than those with 30 degree angle plys. This observation has also been reported by Graves (10). Since such a limited amount of static data is presented, it is possible that this effect is just a manifestation of the scatter normally found in composite properties.

During the tests, popping sounds beginning at loads larger than about 90% of the ultimate static load often warned

that catastrophic failure of the specimen was imminent. Fractures were usually perpendicular to the loading direction and always through the hole. Because most tests were run in load control, testing machine motion after failure caused extensive damage to the fracture surface. Testing some specimens under stroke control eliminated this post-failure damage and resulted in some clean, sharp cracks across the specimen. This indicates delamination was probably not a primary mode of static failure, although Moire observation of the surface of two specimens prior to failure did indicate some local delamination at the hole edge.

5.2 FATIGUE LIFE DATA

Figure 7, plotted from data in Tables 2a through 2d, illustrates the fatigue life behavior of the four laminate types investigated in this program. Results of the static tests, plotted close to the vertical axis and represented by the smaller symbols, are also presented. A majority of tests were conducted with ($\pm$45/0)s specimens 21 cycled to failure and 26 stopped prior to failure. None of the ($\pm$45/0)s specimens suffered a fatigue failure when tested at a maximum compressive load less than 300 MPa. Samples tested at lower loads survived a minimum of 600,000 cycles, with two tests extended to one million cycles with no failure.

A smaller amount of data, 16 points in all, represent the fatigue failures of the three other laminate types tested. The data from the (0/+45)s fatigue tests are particularly interesting. While the static strength of this layup was found to be nearly identical to the (+45/0)s laminate's, the fatigue life was significantly lower. One specimen tested at 276.1 MPa failed after only 40,000 cycles. This, along with the rest of the data for this laminate, indicates that a stacking sequence effect exists for the flawed laminate when subjected to cyclic, but not to static, loads.

No stacking sequence effect can be observed in the limited amount of (+30/0)s and (0/+30)s data. When tested at the same load levels, failures of both laminate types were intermixed within a comparatively small life range.

5.3   RESIDUAL STRENGTH DATA

The residual strengths for 17 of the (+45/0)s specimens which survived cyclic loading are listed in Table 2b. These data points, along with the static strength data for this layup, are plotted in Figure 8. Later sections of this report will show that many of these specimens had developed extensive areas of delamination prior to the residual strength test. Even with this visible damage, however, only a slight reduction in load carrying ability from the static strength distribution can be seen after fatigue.

5.4   DAMAGE INITIATION DATA

Measurement of life to first observable fatigue damage
was a major objective of this test program. The results of
damage initiation measurements are listed in Tables 2a
through 2d, with initiation data for all four laminate types
consolidated in Figure 9. The 92 points from (+45/0)s tests
seem to demonstrate a bilinear behavior behavior on this
semi-log plot. Points for damage beginning before 20,000
cycles follow a negatively sloping line down to approxi-
mately 280 MPa, while later initiation data is almost flat.
No damage was found on any specimen tested below 260 MPa, in
two cases even after 1,000,000 cycles.

Damage initiation in the (+30/0)s laminates falls within
the the scatter of the (+45/0)s data. Both laminates with
the unidirectional plys on the outside, however, show signs
of damage significantly sooner than the average time to ini-
tiation for the corresponding laminate with the angle plys
on the outside.

In every specimen showing signs of damage, initiation
occurred at the free edge of the hole. Figure 10, using data
from Tables 2a through 2d, plots the angular position of the
initiation site measured counterclockwise from the loading
direction. Data for each laminate type is plotted on one of
the concentric circles representing the hole edge. Three of
the laminates, (0/+30)s ,(0/+45)s , and (+30/0)s tended to

initiate damage within a 10 degree sector counterclockwise from the perpendicular to the load direction. The (±45/0)s laminate, however, behaved differently. In all but a few cases, initiation for this layup was within ±10 degrees of an intersection between lines ±45 degrees from the load direction and the hole edge. Damage initiation behavior has thus been experimentally shown to depend both on ply orientation and stacking sequence.

5.5 DAMAGE PROPAGATION PHOTOGRAPHS

As described in section 2.3, Moire interferometry was used to observe damage initiation and propagation during fatigue cycling. As many as 150 photographs of the Moire patterns on each sandwich column face were taken as a specimen was tested. Appendix A presents a set of between 3 and 16 individual pictures selected to illustrate the progression of damage for every laminate face which showed a significant amount or growth.

The figures in the appendix have been grouped by laminate type, and within each laminate type are ordered chronologically as tested. Labels below each picture indicate the number of fatigue cycles experienced by the specimen at the time of the photograph. ,The first picture of a group is always at 0 cycles. It shows the background pattern resulting from a slight misalignment between the reference grill and the specimen, as well as some interference caused by the

interaction of the peel-ply textured graphite/epoxy surface and the grill lines. The second picture is a print from the negative showing the first sign of damage when examined at 10x magnification. The last of a series is always the final exposure made prior to failure or the cessation of fatigue loading. In addition, some sets include a few illustrations of damage growth during statically applied loads of the residual strength tests.

Each picture shows an area surrounding the hole in one of a specimen's graphite/epoxy face sheets, viewed from a point along the surface perpendicular located with its origin at the center of the hole. The horizontal dimension of the print approximately covers the width of the specimen, about 5cm. The vertical dimension, corresponding to the direction of the applied load, varies from set to set. Exact dimensions can be determined by using the hole's known diameter of 1.25cm. to scale any measurements. The test number indicated on each figure corresponds to the same number in Tables 2a through 2d, with the letter designating which specimen face is illustrated. Figures with the same number but lettered a and b are the two sides of the same column.

Interpretation of the Moire patterns is simplified if one recalls that each fringe line shows an increment of out-of-plane motion, and each picture represents a contour map of surface displacement in the z direction. Continuous contour

lines indicate subsurface delaminations. Discontinuities in the contour lines occur at locations where through cracks have developed. The pattern visible inside the hole itself resulted from the deformation of the underlying film adhesive into the core's honeycomb cells during beam bonding.

Inspection of the figures of Appendix A reveals several interesting facts. As described in the previous dicussion of Figure 10, the damage initiation site is extremely consistent within a laminate type. Furthermore, the pictures show that each laminate type propagates damage in some characteristic pattern early in its life. For the (+45/0)s laminates, shown in Figures A1a through A41b, damage tends to develop in a four leaf clover shape. Moire patterns indicate that splitting, defined as through the thickness ply failures in the fiber direction, does not usually occur for some time after initiation. Contrast this behavior with that of the (+30/0)s laminates, shown in Figures A44a through A48b. With this layup the small initial area of delamination, located approximately 90 degrees from the load direction, quickly developed splits in the direction of the outer fibers.

Tests of the two laminates with 0 degree plys on the outside, Figures A42a through A43b for the (0/+45)s's and Figures A49a through A54b for the (0/+30)s's showed they initially behaved in a manner similar to that of the (+30/0)s

layup. Once splitting in the load direction began, however, the damage progressed much differently. Splits divided the surface ply of each laminate into narrow regions which buckled to form small arches, each arch having a length of approximately one hole diameter. Continued fatigue cycling caused the $(0/\pm30)$s specimens to develop a stairstep pattern of these arches which propagated in the direction of the angle ply closest to the surface. Since only a few $(\pm45/0)$s specimens were tested, no conclusive statement regarding this laminates behavior after initiation can be made.

Graves (10) has also published data describing damage progression during compressive fatigue of the same four laminates studied in the current program. Surface damage observed during periodic visual inspections was sketched. Similarities between these sketches and the Moire patterns of this report can be seen, particularly during the early stages of development. Later in the specimen's life, however, the results of the two tests show drastically different behaviors. Graves shows propagation along the specimen length, often extending from one end to the other. Damage during the current investigation restricted itself to the immediate vicinity of the hole.

Two possible explanations for this difference are proposed. The sandwich specimens used by Graves contained 0.635cm. diameter holes, half the size of those used in this

program. It is possible that the change in hole size, by reducing the difference between the net section and far field stress, caused visible damage to develop in both regions. Graves far field and net section stresses differ by only 15%. At the net section stress level of his tests, 337 to 358 MPa, his far field stress was above the load found in the current program to produce no damage.

The methods used to introduce the compressive load into the specimens are a second possible source of the observed differences in propagation behavior. The current program employed axially loaded specimens, while Graves used a four point bending technique. By producing a compressive load in this manner, an unwanted curvature is introduced into the test section. The rate and direction of delamination is undoubtably influenced by the concave deformation of the compressive face.

5.6 DAMAGE AREA DATA

For every picture in Appendix A, the area bounded by the outermost fringe line of the Moire pattern was measured by the method described in Section 4.4. The damage areas for all specimens showing a significant amount of propagation have been plotted in Figures 11 through 19, with areas larger than the limit of the scale indicated by an arrow at 4.75cm. Individual data points for each specimen have been connected by straight line segments, and each curve is iden-

tified by the symbol plotted at the location of the last data point measured. In most cases data for both sides of a specimen are presented. It should be remembered that in these load controlled tests, fracture of just one of its sides resulted in the complete destruction of a specimen. When the behavior of the two sides of a specimen are compared, it often seems obvious which side was responsible for the final failure. The assumption that failure was caused by the side with the most rapidly growing damage or the greatest area was not experimentally tested for or verified.

Figures 11 through 13 show data for (+45/0)s specimens that failed during fatigue cycling. Each figure contains the data for a small, arbitrarilly chosen, range of maximum compressive stresses. Most of the (+45/0)s curves can be divided into three regions. Region 1, the nearly horizontal portion, is characterized by the initiation and slow growth of damage. Region 2, represented by a curved transitional section, is an zone of increasingly rapid propagation. The end of this region often corresponds to the onset of major splitting or the coalesence of two smaller damage areas, as shown in Appendix A. Region 3, the nearly vertical section of the curve, usually lasts for a relatively small portion of the specimens life but contains a large percentage of the total damage accumulated during fatigue cycling.

No correlation between damage plots for the two sides of the same specimen can be identified. Sometimes the two curves follow each other closely. At other times damage on one face grows rapidly while little or none developes on the other. Occasionally the two curves cross each other one or more times before failure. The appearence of all three behaviors suggests that no significant interaction between the two faces of a specimen occurred, and each pair of initiation and propagation data can be regarded as coming from two separate tests.

Plots which do not follow the main body of data, those of Tests 52b, 58b, 77a, and 82b for example, begin Region 3 type behavior early in their lives. Some of these same tests are responsible for initiation sites in Figure 10 that lie outside the four leaf clover pattern. This indicates that initiation in these tests probably occurred normally but individual areas had already joined by the time a photograph was taken.

Examination of Figures 11 through 13 shows that maximum damage area does not always correlate with fatigue life or maximum compressive cyclic load. Early failure does not necessarily imply a small final damage area or a high maximum load, as evidenced by test 58b on Figure 13. The trend, though, is definitely toward larger amounts of damage developing on the longest lasting specimens, with relatively small amounts of damage found on those that failed soonest.

The above descriptions also apply to the next two graphs, Figures 15 and 16, which show damage progression in the (±45/0)s tests stopped prior to fatigue failure. Figure 15 contains data for specimens loaded in the maximum compressive load range which had produced fatigue failures in some tests. Notice that several curves on this plot indicate Region 3 type behavior and suggest specimens which are probably nearing failure. In particular, note the damage area of Test 63a, listed as 10.045cm. in Table 2b. The pictures of Appendix A, Figure A30a, show that damage on this specimen had actually propagated to the left edge of the coupon without producing a fatigue failure.

Each of the last three plots of this group, Figure 17 through 19, contain propagation data for both the failed and unfailed specimens of one particular laminate type. Figure 17, showing the (0/±45)s data, indicates only one specimen had developed sufficient damage to be plotted. Others either failed with very small damage areas or were removed from testing soon after damage was observed. The single plot shown does indicate Region 3 behavior occurred immediately after initiation.

The (±30/0)s data in Figure 18 shows this laminate's behavior is very different from the (±45/0)s's. After a short period of slow damage growth, rapid propagation develops with almost no transitional period. Fatigue failures,

indicated by the check marks next to the individual run num-
bers, occurred with relatively little observable damage.

Contrast the (±30/0)s behavior with that of the (0/±30)s
specimens plotted in Figure 19. These laminates, with their
zero degree plys on the surface, show the same three regions
of damage propagation observed in the (±45/0)s specimens.
Region 3 growth is very steep, a result of the stairstep
nature of the damage development (see Figures A49a through
A87b). Damage areas at failure were similar to those of the
(±45/0)s's, and much greater than damage found in the
(±30/0)s tests.

5.7 MICROSCOPIC CROSS SECTION EXAMINATION

Specimens from ten fatigue tests were removed from the
testing machine with various amounts of visible damage, and
cross sections of their laminates observed under 250x magni-
fication. Three different forms of damage were seen. Tight
vertical cracks extending from one ply interface to an adja-
cent interface, probably a result of minor matrix failures,
were the most numerous form. Horizontal spacing of these
vertical cracks varied from only a few in the entire cross
section to as many as 10 per millimeter in areas of heavily
damaged laminates. One laminate that showed no indication
of damage using Moire interferometry contained four of these
vertical cracks in a 2cm. long cross section taken 1mm. from
the hole.

A second form of damage, generally corresponding to areas where Moire patterns were seen during testing, was delamination. This type of damage propagated along ply interfaces, and occasionally jumped from one interface to another through a vertical crack. Parallel growth of two delaminations, one above the other, was only seen in specimens with large amounts of damage. Major concentrations of the one ply long vertical matrix cracks had at least one of their ends extending from delaminations.

Through cracks, major intraply failures visible as splits upon reaching the surface, were the least common type of damage. In all cases these were associated with delaminated areas below the surface.

Damage in $(\pm45/0)$s laminates was most concentrated in the top two surface plys. Delamination usually propagated along ply interfaces, but was ocassionally seen to drift into intraply regions for short distances. In specimens with large amounts of damage, delamination and vertical cracks did develop in the plys near the core, but damage to the film adhesive layer between the graphite/epoxy and honeycomb was never seen. It is important to note that some of these laminates had splits through the zero degree plys, indicating that locally massive fiber reakage in the main load carrying ply could be sustained by a specimen without failure.

Observation of laminates with their angle plys at the center of the specimen showed that very shortly after initiation, damage existed only in these interior plys. A vertical split located at the mininmum net section was found in a specimen that had not yet developed the stairstep damage to the surface zero degree plys.

Figures 20 through 22 contain 50x micrographs of cross sections from three different (+45/0)s specimens. The location of these cross sections corresponds to a cut along a vertical line 0.5mm. to the right of the hole. Because both the contrast and the magnification of these pictures are low, much of the minor damage observable during visual inspection can not be recorded photographically. Sketches of observed damage, drawn during a slow ply by ply scan of the 2cm. long sections at 250x, are therefore also presented. Recall that while only three samples will be described in detail, 20 laminates, each sectioned at two or three locations, were inspected in this manner to provide the background for the previous discussion of damage types.

Figure 20 shows damage sustained by the laminate of Figure A12a after 300,000 cycles. The numbers from -10 to 10 found at the top of the sketch indicate longitudinal position, measured in millimeters, above or below the hole center line. Many fine vertical matrix cracks are seen to have developed in both the inner and outer angle ply pairs, but

delamination, indicated schematically by the heavy areas along ply interfaces, has only occurred in the surface pair. The wide vertical lines in the sketch indicate splits through the thickness of a ply, a more severe form of damage than the much more common matrix cracks. Two such splits were found at this cross section. The photograph shows one of these splits, at location -5 on the sketch, and illustrates a jump of delamination propagation from one interface to another. A similar small split, not yet through to the surface, can be seen forming at the upper right.

The damage seen at this cross section was relatively minor in comparison to laminates showing more growth in their Moire patterns. The approximately 1mm. long delamination located at 0 in the sketch is not visible in the Moire picture of Figure A12a, while the 2.5mm. delamination at -5 can be associated with the small spot on the lower right edge of the hole. This information gives some indication of the minimum delamination size detectable by the Moire interferometry method of inspection as applied in this investigation.

Figure 21 is a cross section of Test 63b, Figure A30b, taken at 1,000,000 cycles. As both the sketch and the Moire pattern indicate, much more damage has developed close to the hole in this specimen than in the previous example. Many vertical cracks, some as closely spaced as 10 per mil-

limeter, were found. Delamination between the upper -45 and 0 degree plys nearly spans the cross section. A shorter delamination between the top ±45 interface also exists. Vertical cracks are most numerous in the -45 degree ply, and connect the parallel delaminations. Two major splits have propagated to the surface, but more importantly, a local failure of the zero degree plys has occurred. This split, located at 3 in the sketch, meets a delamination at the inner -45 ply interface.

A second cross section, taken approximately 0.5cm. to the right of the hole edge, shows much less damage. All forms, including matrix cracking, have been restricted to the top two plys. The two major splits shown in the the cross section closest to the hole are seen to have propagated along the fibers to this location.

The photograph, taken at the cross section nearest the hole, shows the area between 10 and 13 in the sketch. A zero degree fiber break is at the far right, while a major surface split is at the upper left. The complete delamination of the top two 45 degree plys is obvious.

Figure 22 illustrates the laminate of Test 44a, Figure A21a. Moire patterns show damage in this specimen at 400,000 cycles falls somewhere between the two previous examples. Microscopic examination confirmed this observation. This specimen was unusual in that a delamination runs

the length of the cross section between the inner 0 and -45 degree plys. More typical upper ply delaminations, along with a share of matrix cracks and splits, also exist. Failure in the zero degree plys is again indicated, both in the sketch and the photograph. Note that a section of honeycomb core can be seen in the lower left of this picture.

To prevent any false conclusions from being drawn, it should be stated that of the many cross sections examined, only two, both taken very close to the hole, contained zero degree failures. As mentioned above, difficulty in photographically recording the damage in a cross section forced pictures only of laminates with large, easily visible damage areas to be taken. The zero degree breaks were both interesting and obvious, thus accounting for their disproportionate share of the above damage photographs.

5.8 ANALYTICAL STRESS FIELD PREDICTION

A modified version of a computer program developed by Bar-Yoseph (52) was used to calculate the three dimensional stress field near a circular hole in $(\pm 45/0)s$ and $(0/\pm 45)s$ laminates. A second program was written to plot the results of the above analysis in an easily interpretable form. It had been hoped that Bar-Yoseph's analysis, which implicitly assumes individual plys to be composed of homogeneous, orthotropic material, would be useful in predicting the experimentally measured damage initiation sites of the lami-

nates used in this test program. Unfortunately, as observation of the resulting stress field plots will show, gradients in the region very close to the hole are extremely steep, with large changes predicted to occur in a distance corresponding to the diameter of a graphite fiber (0.0076 mm.).

Two important points must be recalled (1) On the scale of this analysis graphite/epoxy is a highly nonhomogeneous material, and (2) the macroscopic stress field near the hole is undoubtedly altered by the microscopic matrix cracks observed to develop prior to and away from the initiation sites of Figure 10. Considering those facts, it is not surprising that observed damage initiation sites did not correspond to the peak stress locations predicted by theory.

The results of this most recent development in the analysis of composite laminate edge layers are none the less of interest to researchers in several related areas, and therefore have been included as Appendix B. Figures B1 through B120 are contour plots of individual stress components calculated on various horizontal planes. These figures present a top view of each plane. Shown is 180 degree sector of the specimen, cut through the hole along a line parallel to the load direction. An area from the hole edge to a radial location just one ply thickness away has been included in the plot. Observation of Figure 20 shows that these plots

span a distance of less than 20 fiber diameters. The incre-
ment between stress contours was chosen to produce 10 cont-
our levels per plot. Results are presented for calculations
performed at five through the thickness locations. Z=1 and
Z=2 are ply interfaces, while Z=0.5, 1.5, and 2.5 are ply
midplanes.

The 60 individual figures for each of the two laminates
analyzed have been divided into two sets. In the first set
of 30, stresses, nondimensionalized by the average far field
axial laminate stress, are presented in the cylindrical
coordinates employed by the analytical method. Figure
titles indicate which stress component is being plotted,
with F used in place of the more traditional 0 as an abbre-
viation for stress. R, T, and Z of course denote radial,
tangential and out-of-plane directions. Note that at the
hole edge the stress free boundary conditions have been
satisfied exactly.

The second set of 30 shows the same data rotated into the
local ply coordinates; 1 is the local fiber direction, 2 is
normal to the fibers and 3 is out of the laminate plane.
FZZ, which is not changed by this transformation, is con-
tained only in the first set. An additional plot, labelled
as COMB in the figures, shows the result of taking the
square root of the sum of the squares of F12, F23, and F31.
This value was calculated in an unsuccessful attempt,

loosely based on the Tsai-Hill failure theory (67), to find some combination of stresses that would have its maximum at a damage initiation site.

Chapter VI

CONCLUSIONS

The location of first observable damage in four different graphite/epoxy laminates has been shown to be an experimentally repeatable layup characteristic. Most of the 92 ($\pm$45/0)s laminates that developed damage during fatigue testing first showed signs of initiation in one of four symmetrically arranged locations around the hole's perimeter. Damage in the other three laminates began within a 10 degree sector measured counterclockwise from the perpendicular to the load direction.

The progression of the damage after initiation was also consistent within a laminate type. Appendix A shows that damage tended to develop in patterns that can be associated with a particular layup. Damage area versus cycle plots for three of the layups can easily be distinguished, one from the other, by their unique individual behaviors in the three regions of growth described by the text. (Insufficient data for (0/$\pm$45)s specimens was obtained to include them in this statement). All three laminate types showed a nearly horizontal region of damage growth (see Figures 11-19) early in their lives. The ($\pm$45/0)s specimens tended to gradually increase their rate of damage growth in a second region.

This transition zone was much less visible on the plots of the two laminate types with 30 degree angle plys. A third period in the damage progression for all three laminates was the region of very rapid propagation shortly before failure. The damage area at failure of the ($\pm$30/0)s's was significantly smaller than that of the other two laminate types.

An important experimental result was the lack of correlation, in all but the broadest sense, between final damage area and either maximum fatigue load or life. In all four laminates tested, a majority of the compressive load was carried by the zero degree plys. Post-fatigue inspection showed damage concentrated mainly in the angle plys. This suggests that better correlation between damage area and load may be found in tests of laminates that initiate and propagate damage in their load carrying plys.

Many specimens showed a rapid growth of damage area immediately prior to failure. This result suggests that some warning of imminent specimen fracture may be obtained by the periodic monitoring of fatigue damage, with emphasis placed on the rate of change of damage growth rather than its physical size.

... forty ($\pm$45/0)s cross sections, taken at different ... with respect to the hole and from laminates showing ... of damage in their Moire patterns, have ... sible sequence of damage propagation

for this type of laminate has been developed from these observations. Initial damage in a ply takes the form of vertical matrix cracks which originate either from high static loads (first cycle damage) or fatigue cycling. These cracks, which almost always stop at ply interfaces, act as nucleation sites for delamination by perturbing the already large interlaminar stresses that occur at these locations. Delaminations then grow to a size where a ply, weakened by the combination of wear-out type fatigue damage and lack of support from adjoining plys, can no longer carry the maximum applied load and splits along the fibers. The load carried in the split ply must be transfered to other lamina, further accelerating damage propagation and producing the Region 3 type behavior described in the previous section.

Moire interferometry proved to be a simple, quick and effective method for the detection of subsurface damage in a composite material. Microscopic examination of damaged specimens showed that delaminations with a length of approximately 2mm. could be routinely detected in the top few plys of the laminate. The method was less useful in the detection of cracks and splits, since these forms of damage do not tend to produce out-of-plane thickness changes. Since the patterns produced are visible to the naked eye, real time observation of damage propagation is possible. This characteristic of Moire interferometry gives it an obvious advantage over many of the more commonly employed composite inspection methods, especially in experiments of this type.

An analysis of the three dimensional stress field near the hole was unable to predict the damage initiation sites of two of the laminates tested. Because graphite/epoxy is highly nonhomogeneous on the scale of the analysis, its failure was not surprising. It seems that an even more complicated approach, taking into account the material's inherent inhomogeneity, will be required to accurately predict initiation sites in an arbitrarily stacked laminate.

LAMINATE TYPE	NET SECTION COMPRESSIVE ULTIMATE (MPa)	E LAMINATE MODULUS (GPa)		R LINEAR REGRESSION CORRELATION COEFICIENT	
		Face A	Face B	Face A	Face B
(±45/0)s	480.6	—	—	—	—
(±45/0)s	493.8	—	—	—	—
(±45/0)s	430.8	—	—	—	—
(±45/0)s	465.6	—	—	—	—
(±45/0)s	—	56.0	—	.9997	—
(±45/0)s	—	52.5	—	.9996	—
(±45/0)s	—	54.8	—	.9996	—
(±45/0)s	496.6	55.6	56.2	.9996	.9997
(±45/0)s	434.2	55.7	57.7	.9999	.9999
(±45/0)s	385.7	51.6	51.4	.9997	.9998
(0/±45)s	469.1	—	61.8	—	.9998
(0/±45)s	417.8	—	53.2	—	.9998
(0/±45)s	473.3	—	56.7	—	.9998
(±30/0)s	404.7	81.6	75.6	.9999	.9999
(±30/0)s	446.2	89.9	81.1	.9998	.9999
(0/±30)s	405.5	81.5	80.7	.9999	.9999
(0/±30)s	399.1	80.3	80.5	.9999	.9999

— not measured

TABLE 1a   STATIC TEST DATA

LAMINATE TYPE	NET SECTION COMPRESSIVE ULTIMATE (MPa)	STANDARD DEVIATION (MPa)	E LAMINATE MODULUS (GPa)	STANDARD DEVIATION (MPa)	LAMINATE THEORY MODULUS (GPa)
(±45/0)s	455.3	40.4	54.6	2.2	54.1
(0̄/±45)s	453.4	30.9	57.2	4.3	54.1
(±30/0)s	425.5	29.3	82.1	5.9	75.8
(0̄/±30)s	402.3	4.5	80.8	0.5	75.8

TABLE 1b   AVERAGE STATIC VALUES

TEST #	NET SECTION STRESS (MPa)	CYCLES TO FAILURE	CYCLES TO DAMAGE INITIATION		FINAL DAMAGE AREA (CM2)		DAMAGE INITIATION SITE (DEGREES)	
			Face A	Face B	Face A	Face B	Face A	Face B
10	400.4	2280	800	800	.916	.381	90	120
12	397.1	19800	800	200	1.077	1.923	131	230
15	394.8	-	-	-	-	-	-	-
5	387.5	4640	500	500	.974	.703	236	313
2	385.5	98250	500	500	2.948	2.361	130	138
13	385.0	63530	1250	2000	2.168	.845	231	227
8	384.4	109180	1400	400	1.800	6.619	138	225
16	383.7	4180	1000	400	.361	.761	229	53
9	382.4	195990	1600	400	3.826	3.519	145	305
40	366.9	16850	4500	1250	.542	.813	325	290
82	365.7	18540	1500	800	1.135	3.046	45	75
41	363.5	5690	1250	5500	.373	-	255	225
86	358.3	137790	1500	400	1.187	1.748	50	310
14	350.6	211530	4500	2500	5.581	.484	42	46
83	344.5	516400	4500	3000	4.084	2.794	257	230
75	341.6	73000	3000	1000	.877	.613	48	45
39	336.0	691140	7500	9500	7.760	1.322	220	125
38	335.5	197390	8000	6500	2.314	1.443	120	310
77	330.8	39620	6000	200	3.084	.626	316	47
58	317.6	80330	5000	1750	1.071	4.581	216	80
52	316.6	182620	17000	7000	.994	3.378	43	120
61	299.8	592950	130000	7000	.432	2.645	40	325

- not measured

TABLE 2a (±45/0)s FATIGUE TEST DATA - FAILED SPECIMENS

TEST #	NET SECTION STRESS(MPa)	CYCLES TO END OF FATIGUE LOADING	CYCLES TO DAMAGE INITIATION		FINAL DAMAGE AREA(CM2)		DAMAGE INITIATION SITE(DEGREES)		RESIDUAL STATIC STRENGTH (MPa)
			Face A	Face B	Face A	Face B	Face A	Face B	
6	348.4	300000	1000	2500	0.529	2.755	230	225	444.1
1	346.1	300000	200	nd	2.595	nd	45	nd	408.7
81	324.4	600000	3250	2000	0.871	1.555	130	47	481.2
63	323.5	1000000	14000	9000	10.045	4.374	42	310	*
79	310.3	600000	6000	60000	0.742	0.884	48	230	471.9
36	306.7	420000	6500	nd	0.942	nd	45	nd	*
35	305.9	660000	120000	35000	0.632	1.077	318	51	*
34	303.7	300000	32500	19000	0.761	1.239	48	225	*
37	298.8	600000	85000	140000	0.510	0.516	41	120	457.5
45	292.6	600000	220000	nd	0.097	nd	325	nd	379.9
43	292.1	600000	20000	380000	1.058	0.190	304	220	427.7
47	291.1	600000	42500	50000	0.097	.120	320	295	427.1
46	284.4	600000	340000	14000	0.535	.556	310	210	447.8
78	282.8	600000	6000	11000	1.548	1.155	153	226	366.7
44	282.7	401210	20000	45000	2.058	.788	237	43	*
69	282.6	420000	95000	35000	nm	.120	315	223	*
48	276.4	600000	nd	40000	nd	nm	nd	40	*
80	275.9	600000	50000	80000	0.890	0.232	46	40	377.7
50	275.7	600000	nd	nd	nd	nd	nd	nd	462.0
51	274.0	600000	270000	170000	0.284	nm	129	218	420.1
49	265.0	600000	nd	190000	nd	nm	nd	310	403.3
71	262.1	600000	115000	320000	nm	nm	230	130	*
53	261.3	600000	nd	230000	nd	.056	nd	45	442.0
54	254.1	600000	nd	nd	nd	nd	nd	nd	427.6
59	249.7	600000	nd	nd	nd	nd	nd	nd	375.0
42	249.5	1000000	nd	nd	nd	nd	nd	nd	398.5

nd   no visible damage
nm   damage area not measured
*   specimen reserved for microscopic examination

TABLE 2b   (±45/0)s FATIGUE TEST DATA - UNFAILED SPECIMENS

LAMINATE TYPE	TEST#	NET SECTION STRESS(MPa)	CYCLES TO FAILURE	CYCLES TO DAMAGE INITIATION		FINAL DAMAGE AREA(CM2)		DAMAGE INITIATION SITE(DEGREES)	
				Face A	Face B	Face A	Face B	Face A	Face B
(0/±45)s	64	344.7	910	nd	nd	nd	nd	nd	nd
(0/±45)s	65	323.6	6040	2000	2250	.016	0.226	100	105
(0/±45)s	70	276.1	40059	37500	5000	nm	2.387	282	95
(±30/0)s	55	398.8	1	-	-	-	-	-	-
(±30/0)s	56	311.6	59310	37500	-	.574	.084	282	280
(±30/0)s	76	289.8	71590	nd	25000	nd	-	nd	275
(±30/0)s	57	286.4	227960	140000	9000	0.587	.813	275	274
(±30/0)s	68	276.6	476550	170000	170000	.232	.477	100	280
(0/±30)s	73	290.0	478090	1250	4500	3.187	0.065	271	275
(0/±30)s	60	275.8	155250	26000	13000	.111	2.329	91	95
(0/±30)s	67	275.7	464140	22500	25000	7.039	1.419	92	273

nd   no visible damage
nm   damage area not measured
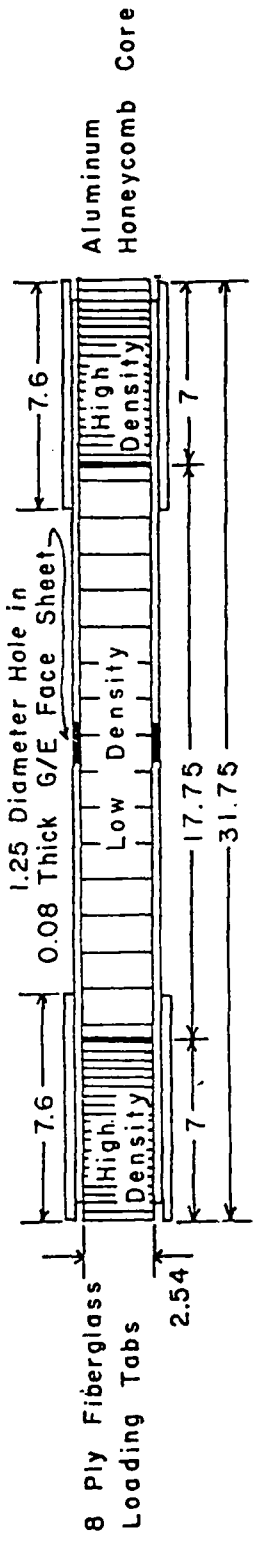
TABLE 2c   (0/±45)s , (±30/0)s and (0/±30)s FATIGUE FAILURE DATA

LAMINATE TYPE	TEST#	NET SECTION STRESS(MPa)	CYCLES TO END OF FATIGUE LOADING	CYCLES TO DAMAGE INITIATION		FINAL DAMAGE AREA(CM2)		DAMAGE INITIATION SITE(DEGREES)	
				Face A	Face B	Face A	Face B	Face A	Face B
(0/+45)s	85	262.2	15000	nd	15000	nd	.232	nd	280
(+30/0)s	74	282.4	170000	120000	37500	.581	.129	95	91
(+30/0)s	89	282.6	220000	65000	220000	nm	nm	233	nm
(0/+30)s	87	282.6	15000	12000	11000	nm	nm	90	275
(0/+30)s	84	282.4	100000	2750	10000	nm	.219	90	270
(0/+30)s	72	276.0	680000	9000	2250	2.032	1.258	90	275

nd   no visible damage
nm   damage area not measured

Test 72 Residual Static Strength = 372.2 MPa
Specimens for all other tests sectioned and microscopically examined.

TABLE 2d   OTHER (0/+45)s, (+30/0)s and (0/+30)s FATIGUE TEST DATA

FIGURE I   SANDWICH COLUMN TEST SPECIMEN

ALL DIMENSIONS IN
CENTIMETERS
NOT TO SCALE
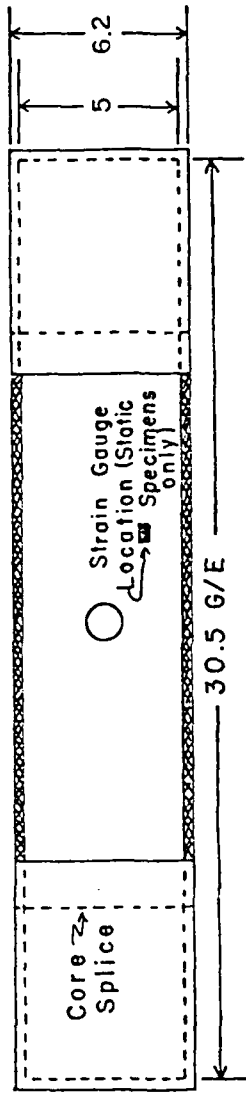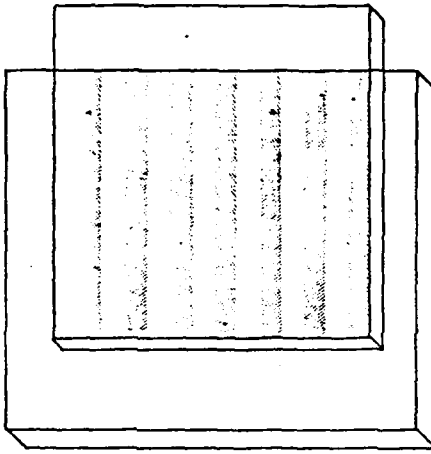
FIGURE 2   MOIRE TECHNIQUE FOR IN-PLANE STRAIN MEASUREMENT
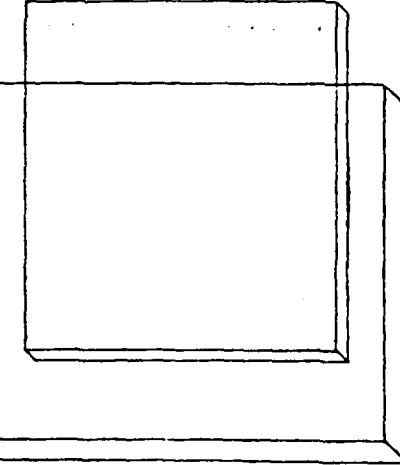
FIGURE 2a

Test specimen with
attached grill of
equal width lines
and spaces

FIGURE 2b
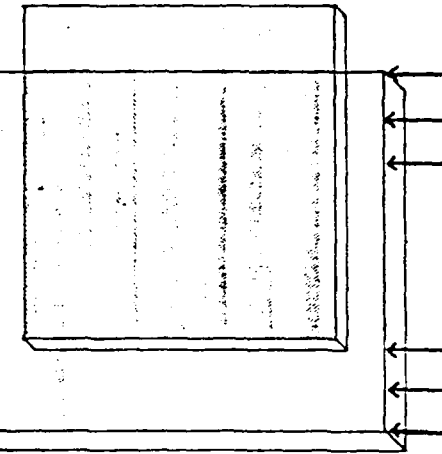
Glass reference
grill with identical
pattern of lines

No interference

FIGURE 2c

Reference shifted
1 line width

Region of destructive
interference developes
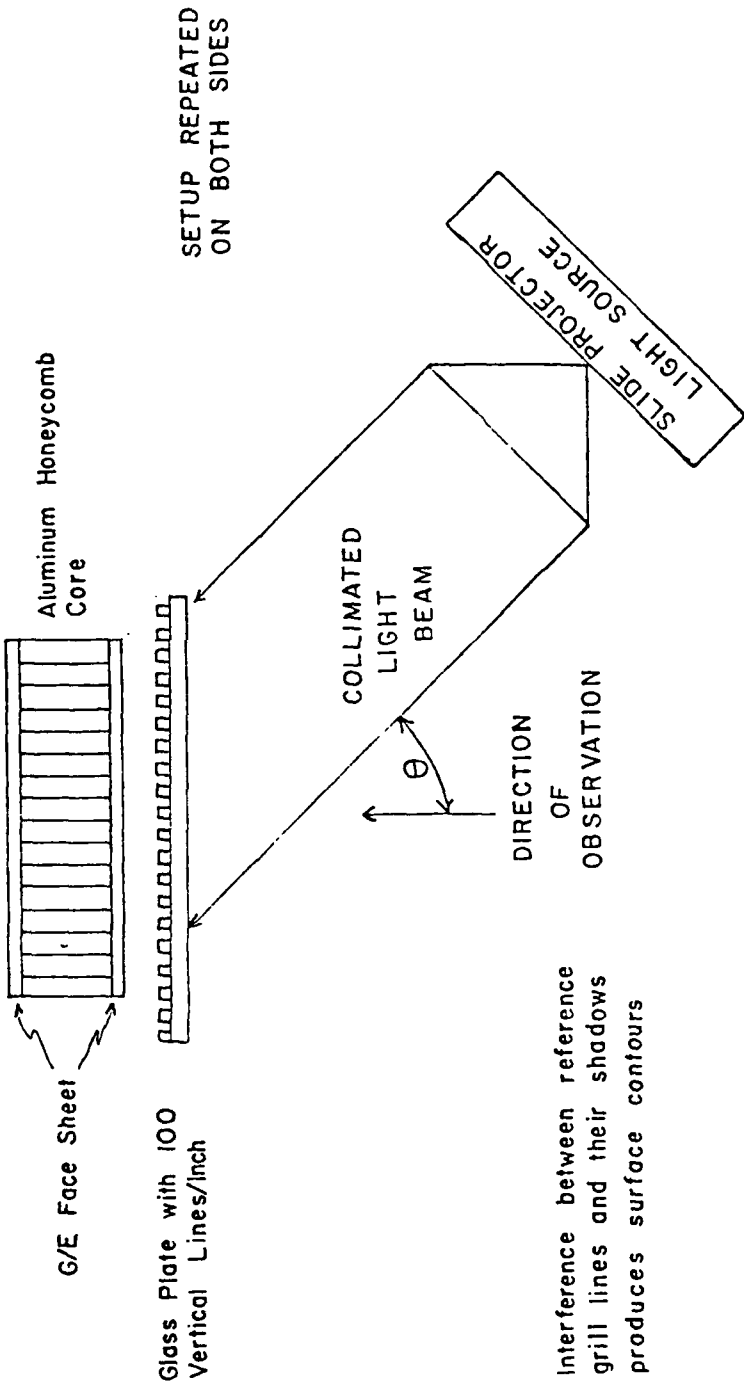
FIGURE 2d

Specimen loaded

Grill spacing
change causes
Moire pattern

FIGURE 3   MOIRE TECHNIQUE FOR SURFACE CONTOUR GENERATION

TOP VIEW OF EXPERIMENTAL SETUP

Aluminum Honeycomb Core

G/E Face Sheet

Glass Plate with 100 Vertical Lines/Inch

COLLIMATED LIGHT BEAM

SLIDE PROJECTOR LIGHT SOURCE

SETUP REPEATED ON BOTH SIDES

θ

DIRECTION OF OBSERVATION

Interference between reference grill lines and their shadows produces surface contours
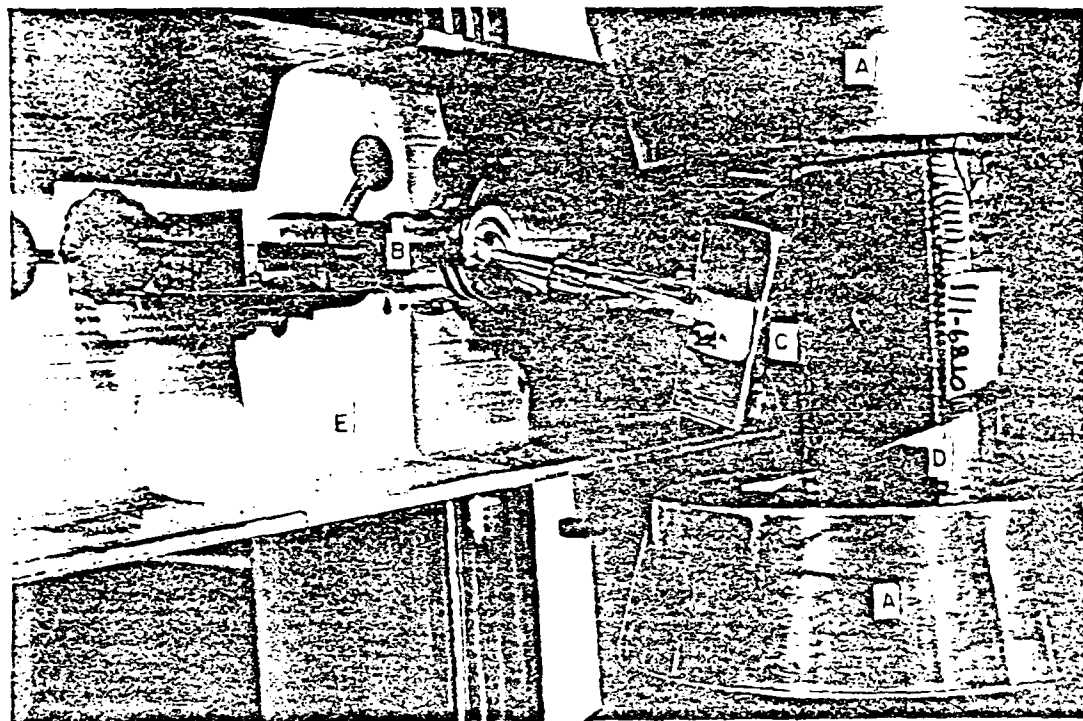
A) TESTING MACHINE HYDRAULIC GRIPS
B) SIX DEGREE OF FREEDOM MOUNT
C) 100 LINE/INCH MOIRE GRILL
D) TEST SPECIMEN
E) VIBRATION ISOLATION MOUNTING

FIGURE 4   MOIRE GRILL MOUNTED NEAR SPECIMEN
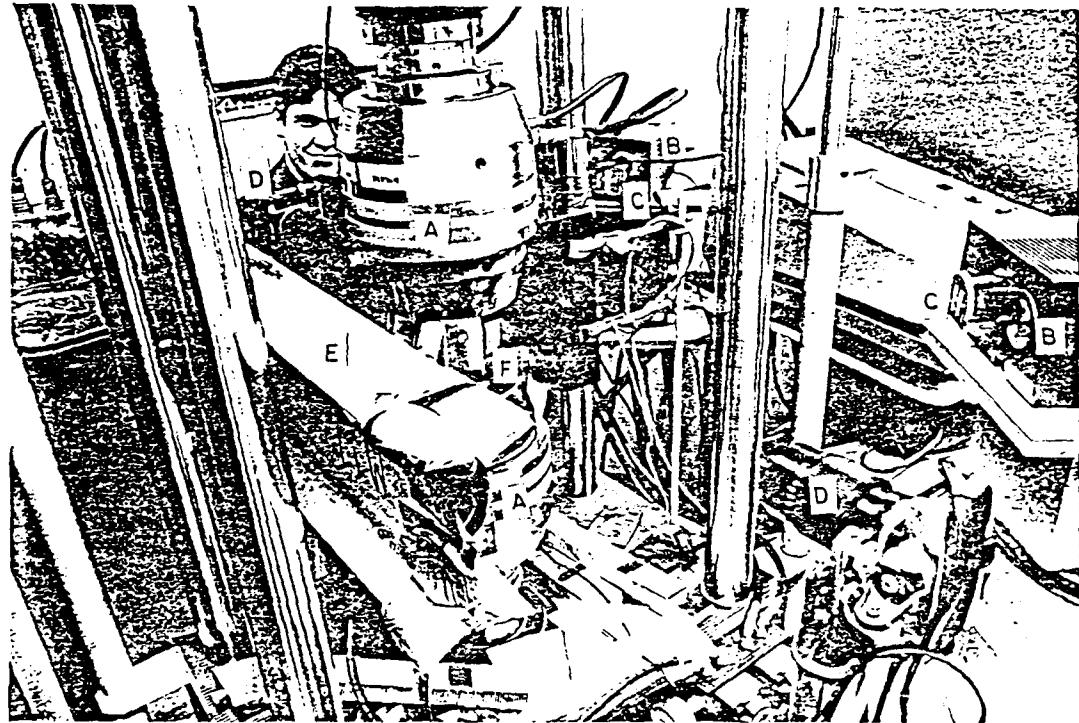
A) HYDRAULIC GRIPS

B) 500 WATT SLIDE PROJECTOR

C) ZOOM LENS WITH KNIFE EDGE SLIT

D) CAMERA

E) VIBRATION ISOLATION MOUNTING

F) SPECIMEN AND MOIRE GRILL

FIGURE 5   EXPERIMENTAL SETUP

FIGURE 6   FAR FIELD STRESS VERSUS STRAIN
TYPICAL OF STATIC TEST DATA
(±45/0)₅ SPECIMEN
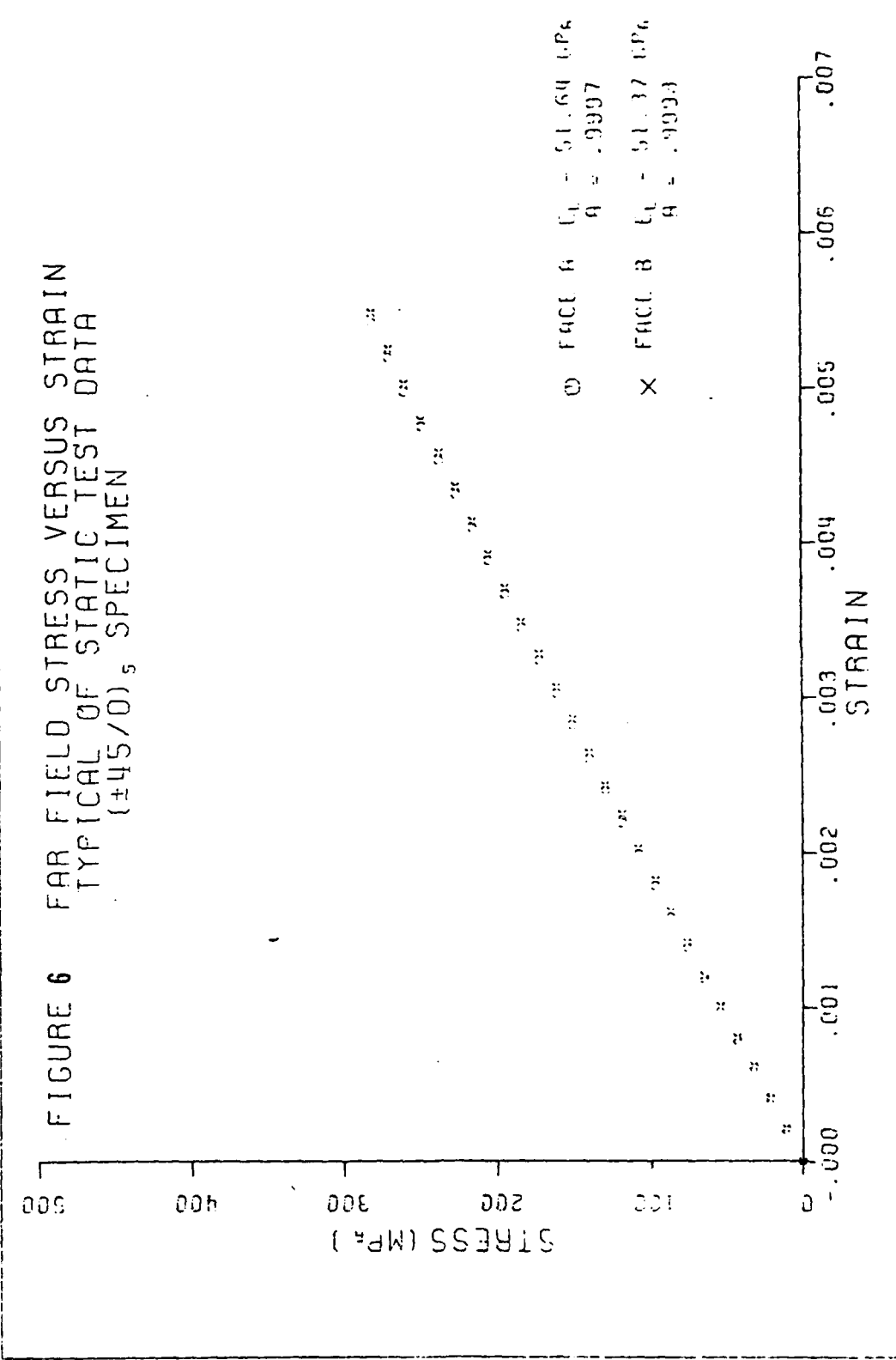
FIGURE 7 NET SECTION STRESS VERSUS CYCLES TO FATIGUE FAILURE
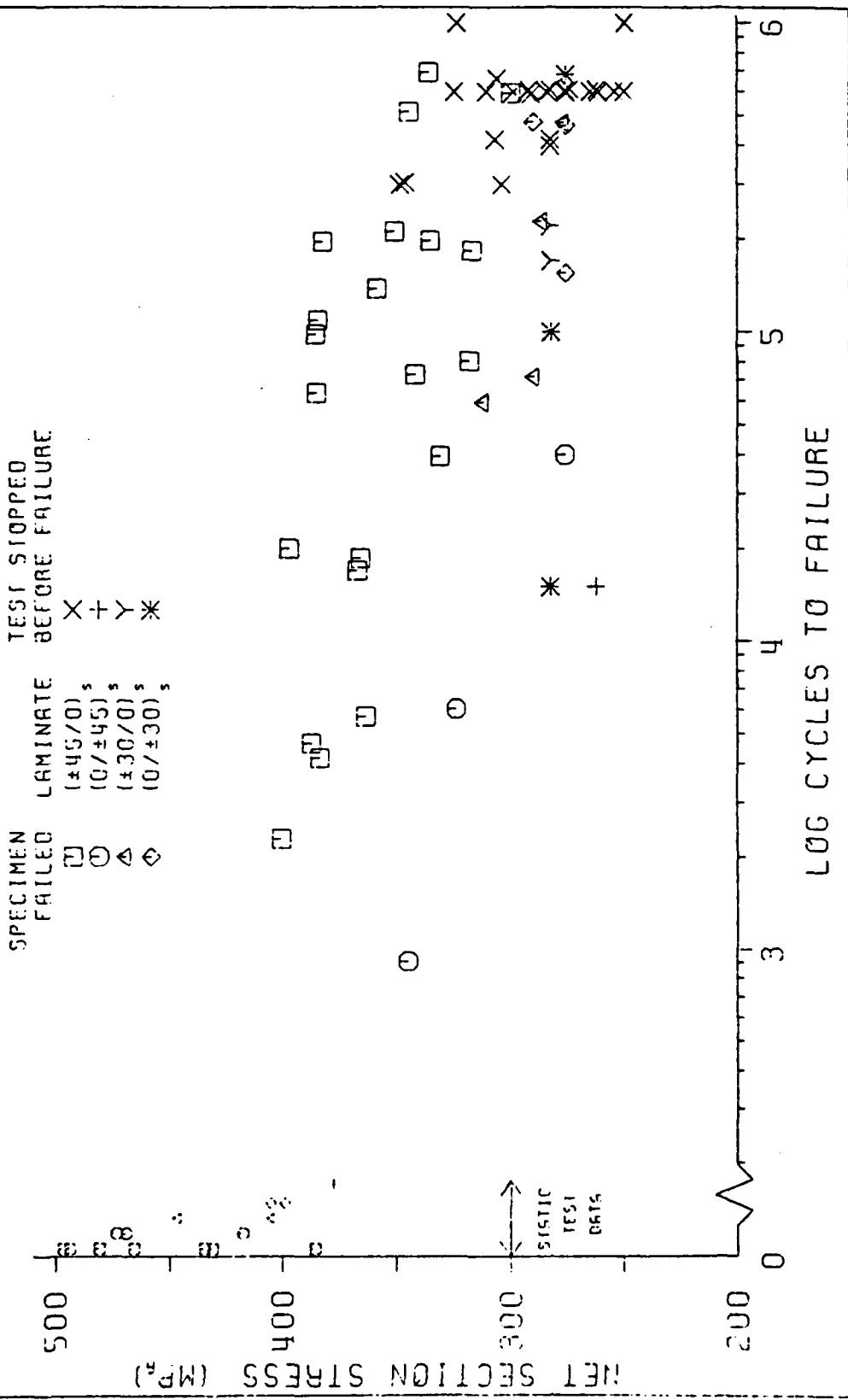
FIGURE 8 (±45/0)$_s$ RESIDUAL STRENGTH VS. MAXIMUM COMPRESSIVE FATIGUE STRESS
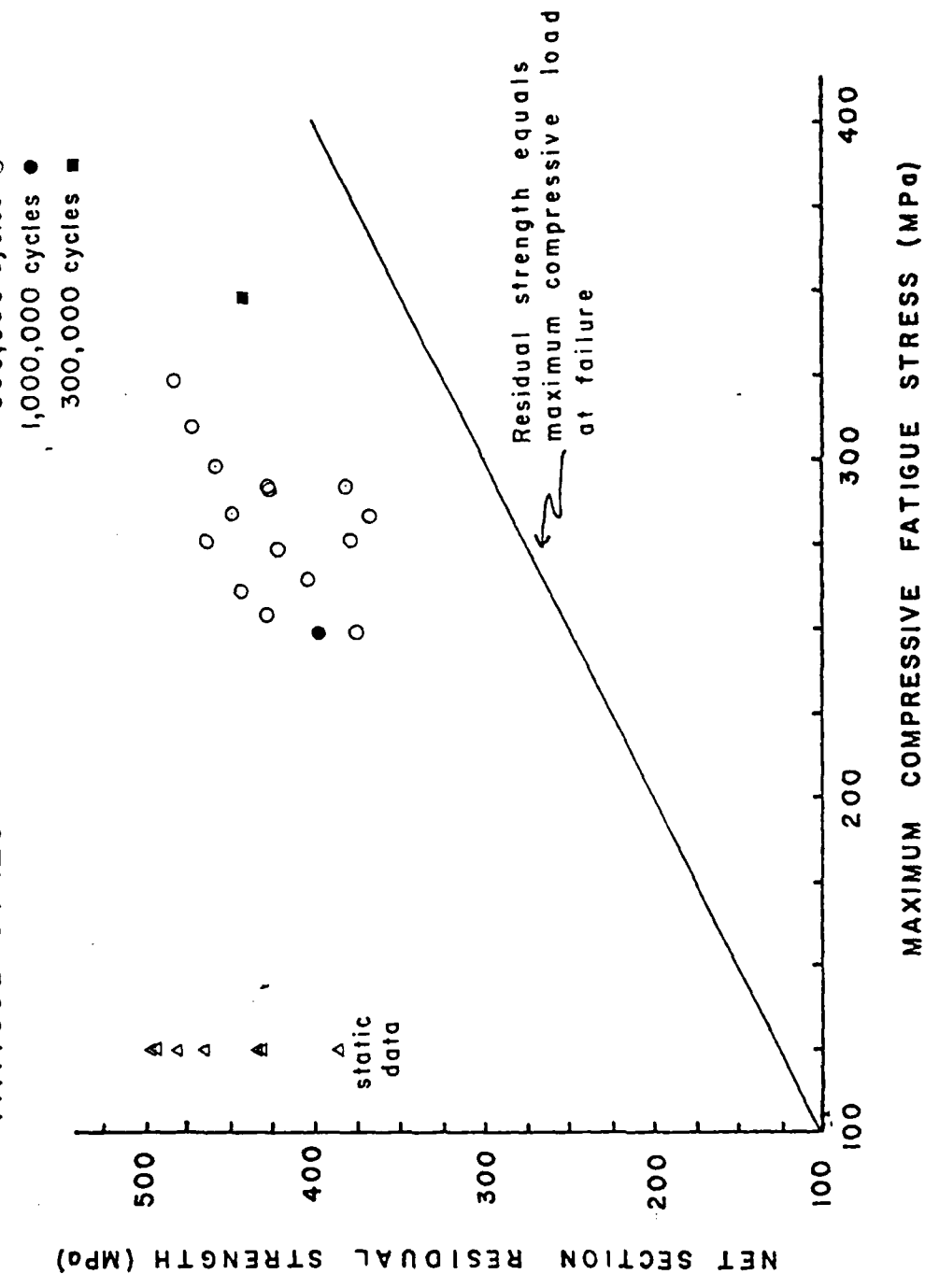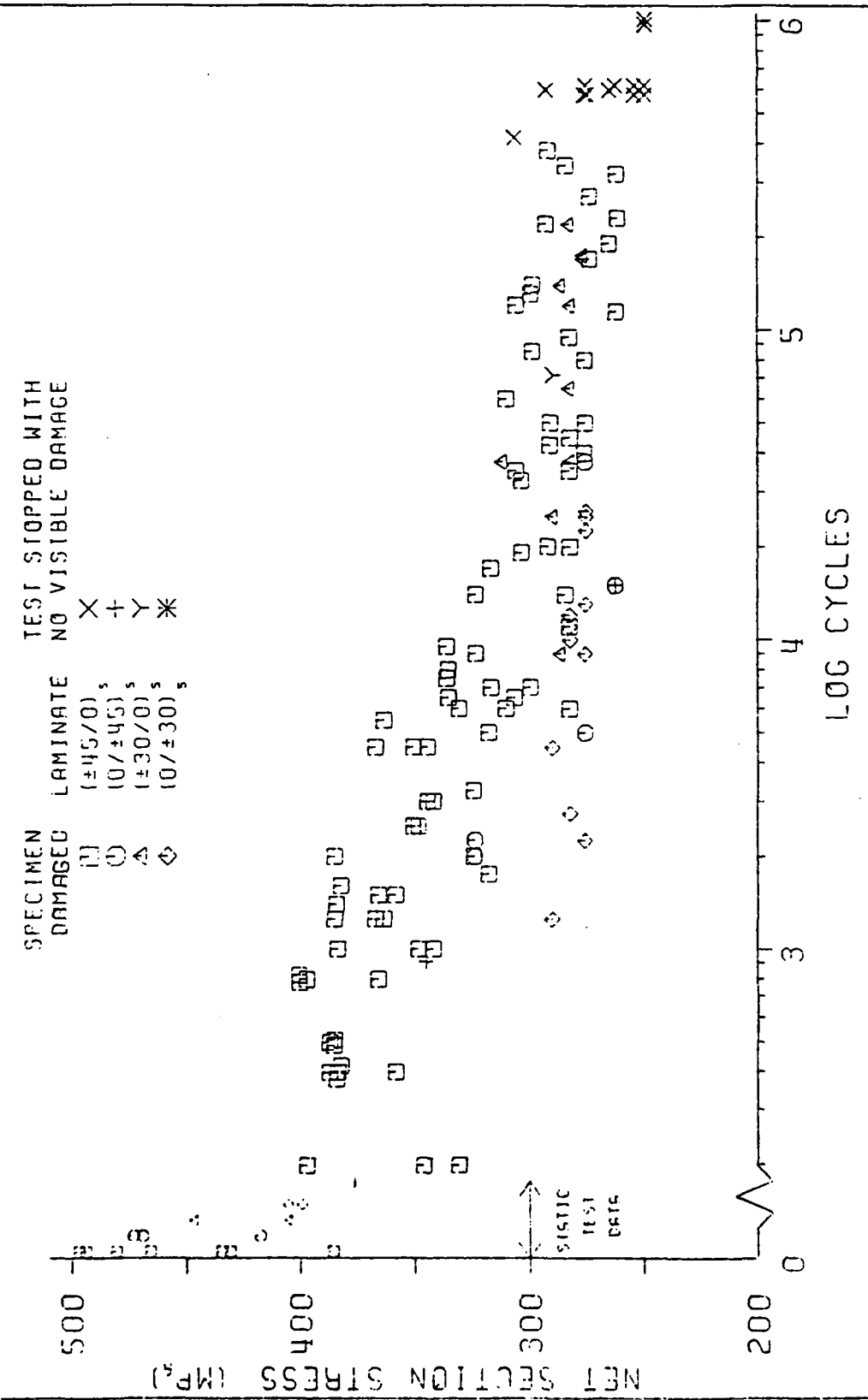
FIGURE 9 NET SECTION STRESS VERSUS CYCLES TO FIRST DAMAGE
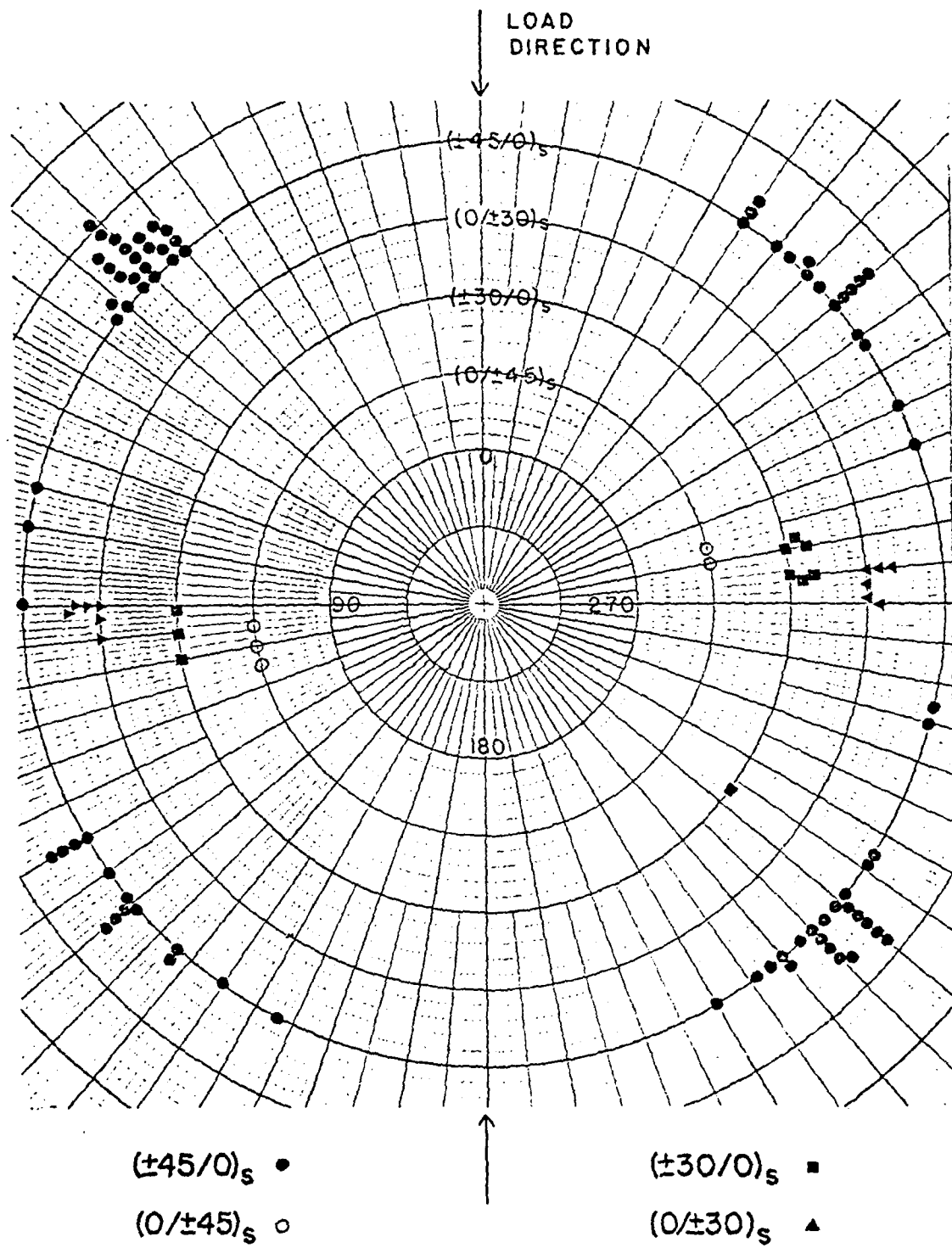
FIGURE 10   DAMAGE INITIATION SITES ON HOLE EDGE

FIGURE 11 DAMAGE AREA VERSUS CYCLES (±45/0)ₛ FATIGUE FAILURES
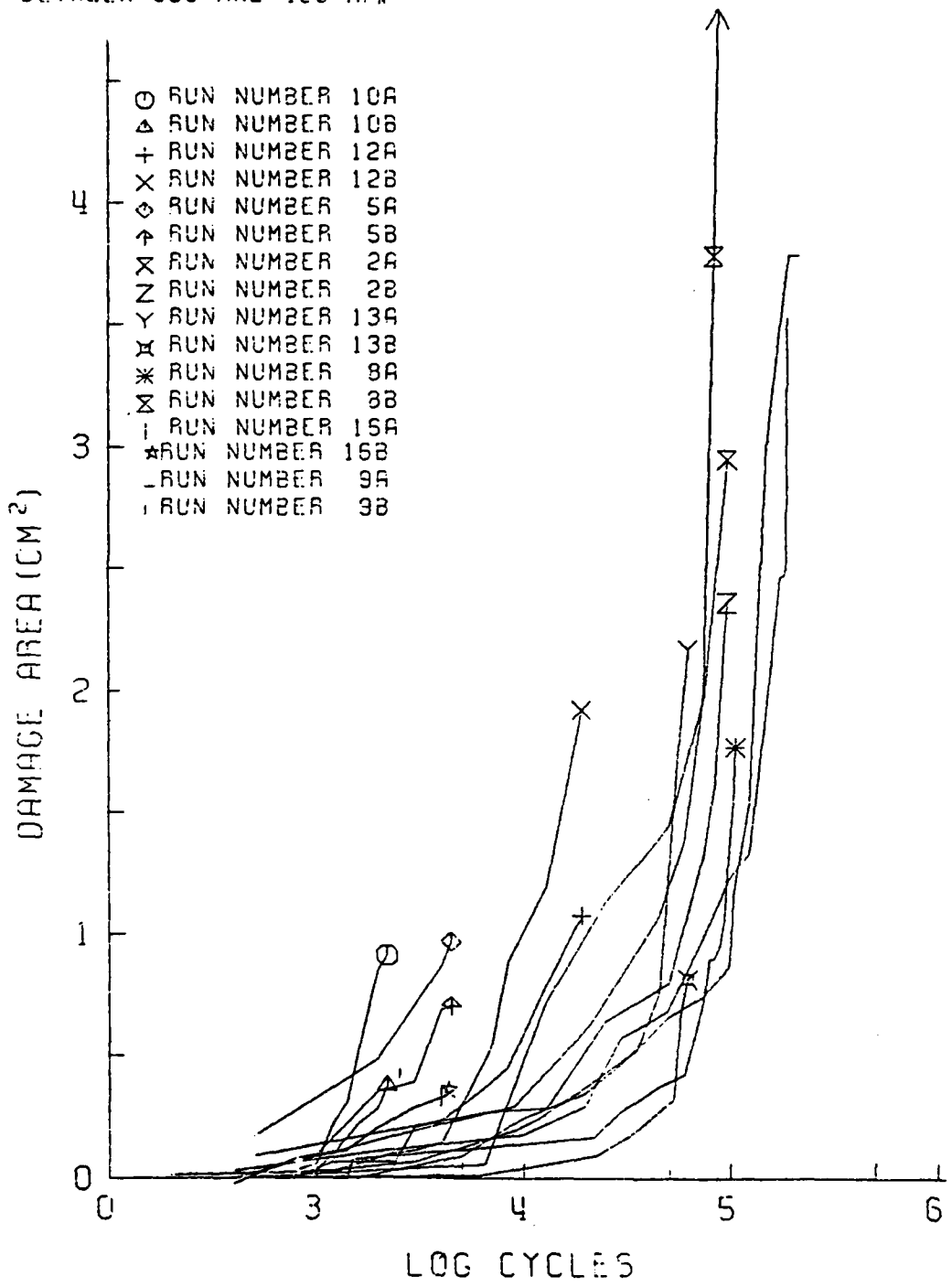
FIGURE 12   DAMAGE AREA VERSUS CYCLES
$(\pm45/0)_5$ FATIGUE FAILURES

DATA FOR MAXIMUM COMPRESSIVE LOADS
BETWEEN 350 AND 370 MPa
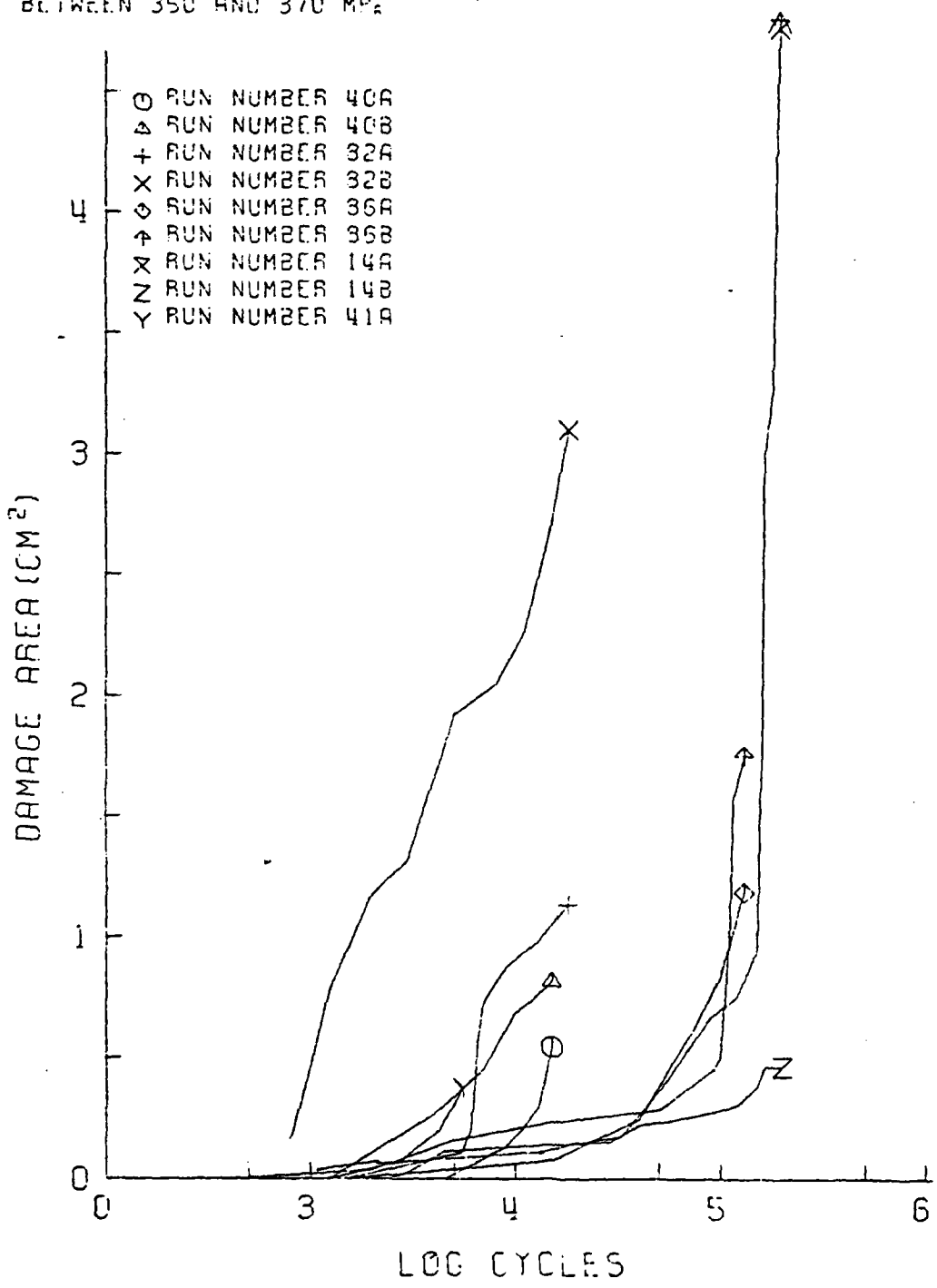
FIGURE 13 DAMAGE AREA VERSUS CYCLES
(±45/0)s FATIGUE FAILURES
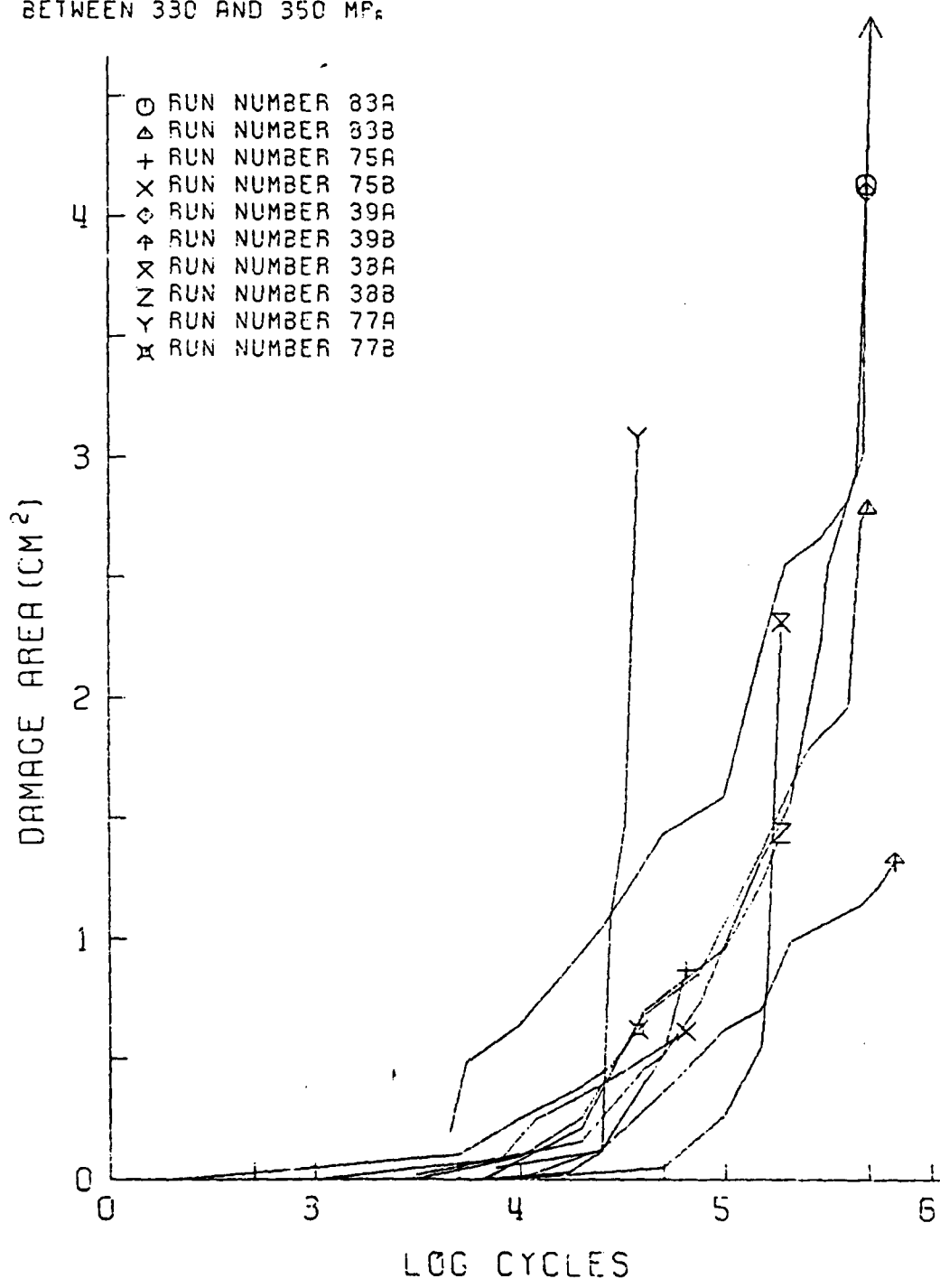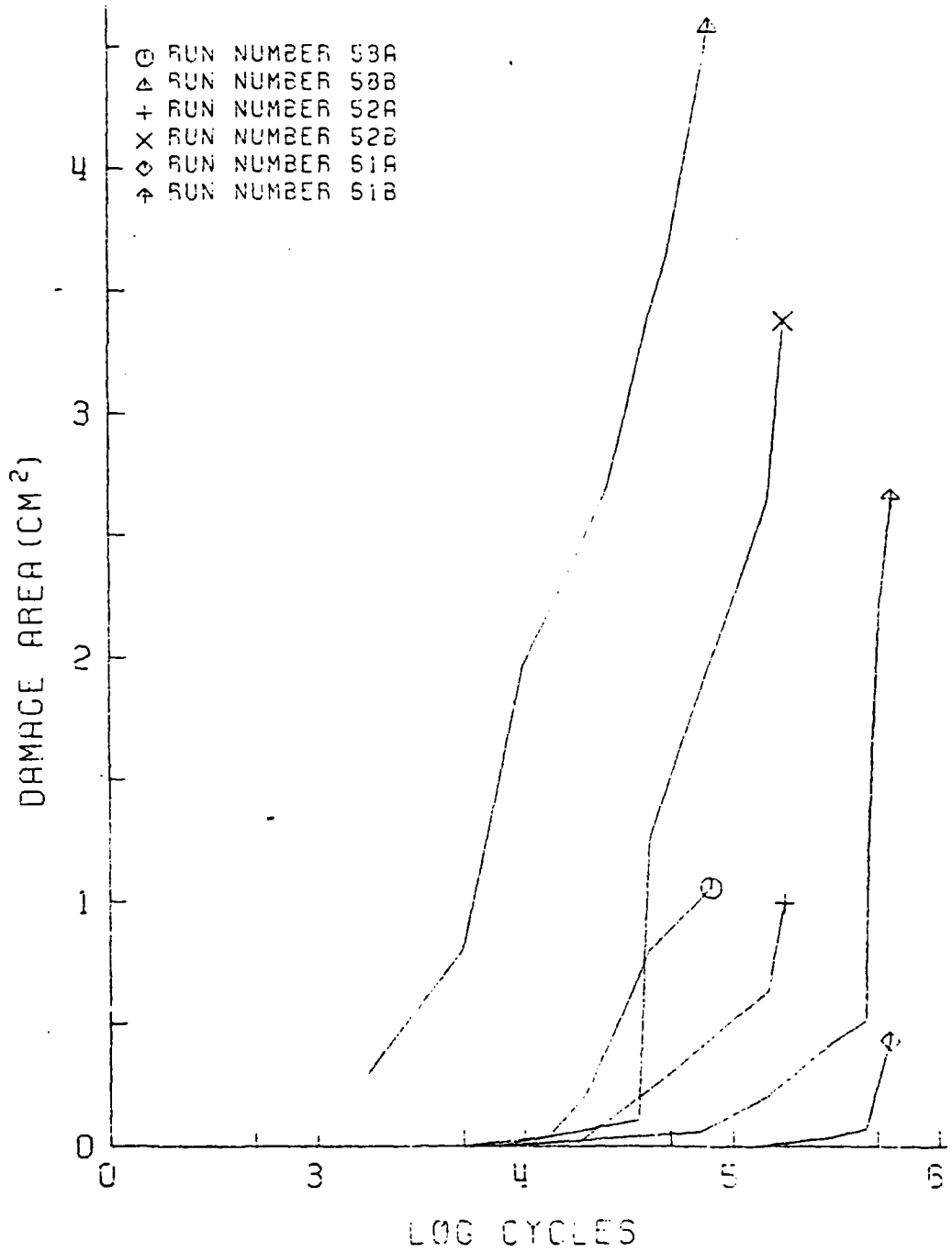
FIGURE 14   DAMAGE AREA VERSUS CYCLES
$(\pm 45/0)_s$ FATIGUE FAILURES

DATA FOR MAXIMUM COMPRESSIVE LOADS
BETWEEN 300 AND 320 MPa

FIGURE 15   DAMAGE AREA VERSUS CYCLES
(±45/0)₅ FATIGUE TEST – UNFAILED SPECIMENS
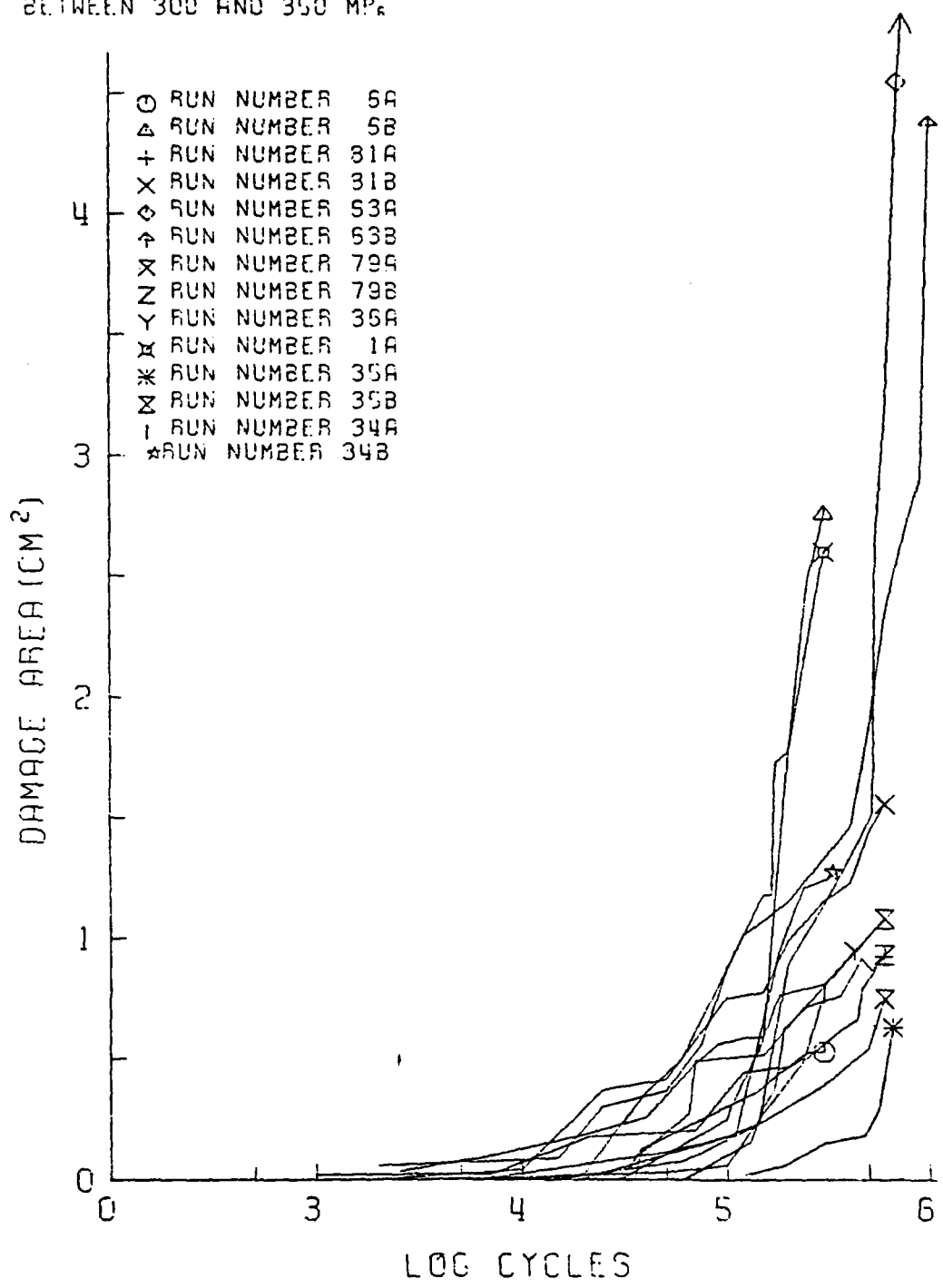
FIGURE 16   DAMAGE AREA VERSUS CYCLES
(±45/0)$_S$ FATIGUE TEST - UNFAILED SPECIMENS

DATA FOR MAXIMUM COMPRESSIVE LOADS
BETWEEN 200 AND 300 MPa
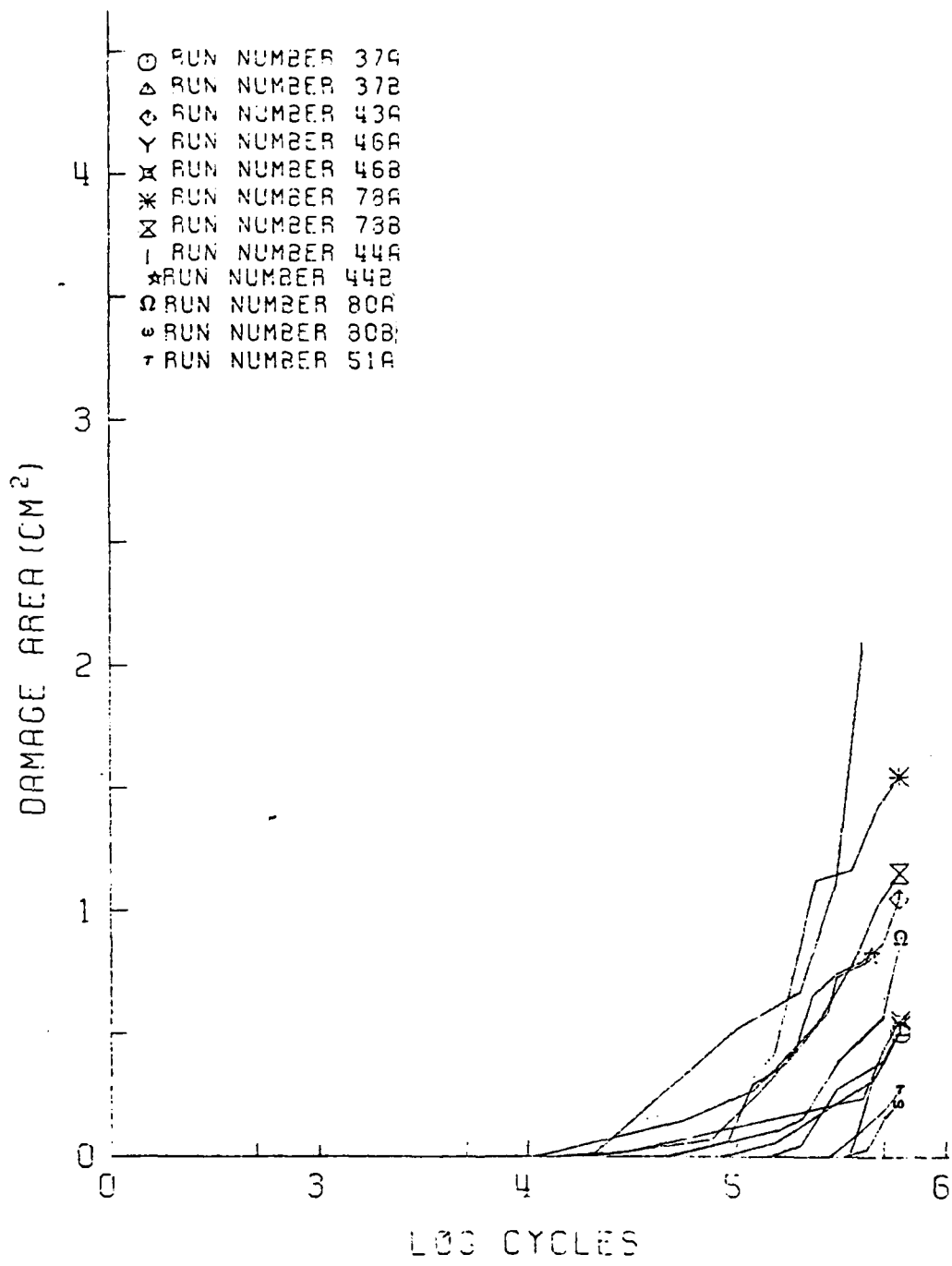
FIGURE 17 DAMAGE AREA VERSUS CYCLES
(0/±45)$_s$ FATIGUE TEST DATA

DATA FOR MAXIMUM COMPRESSIVE LOADS
BETWEEN 260 AND 325 MPa
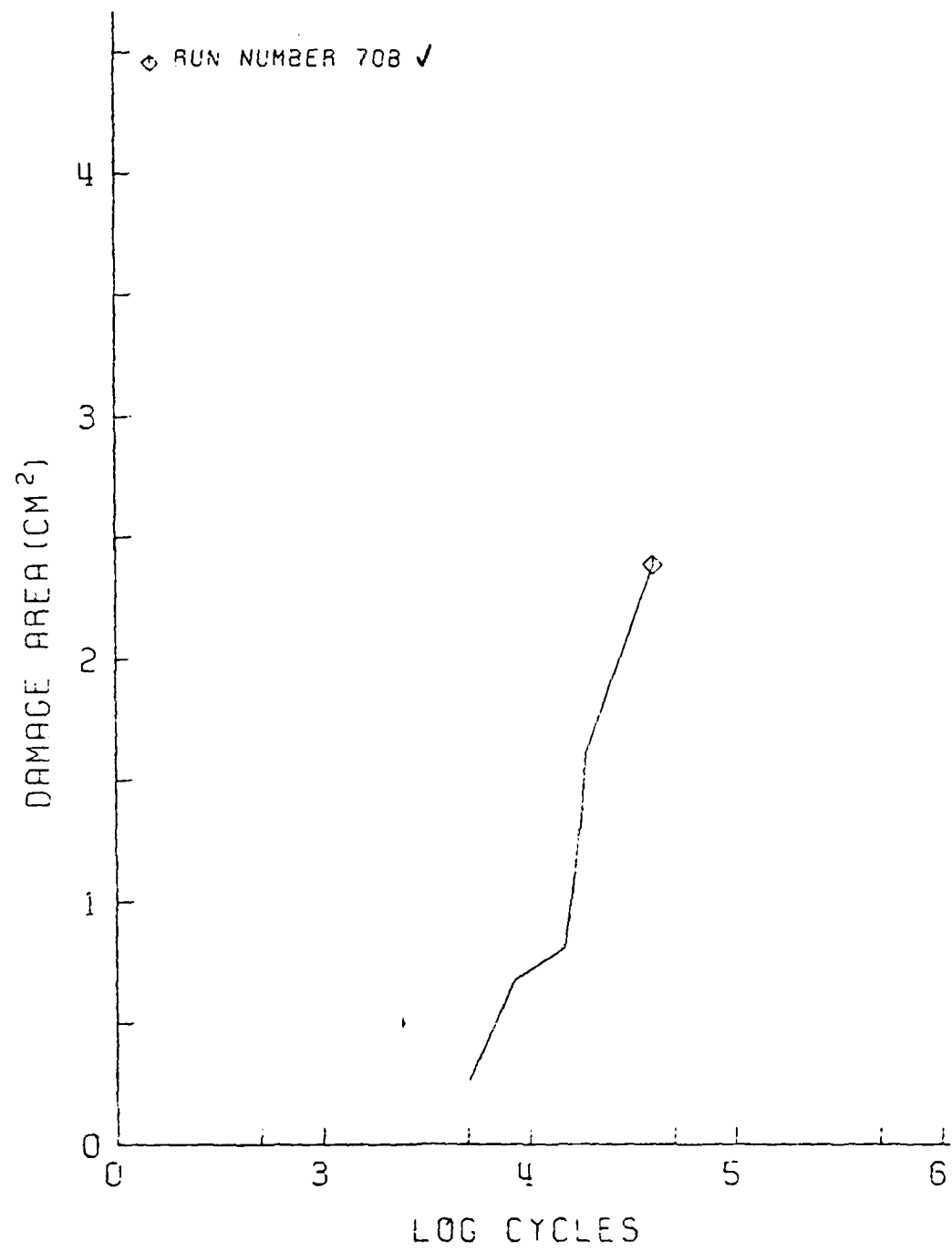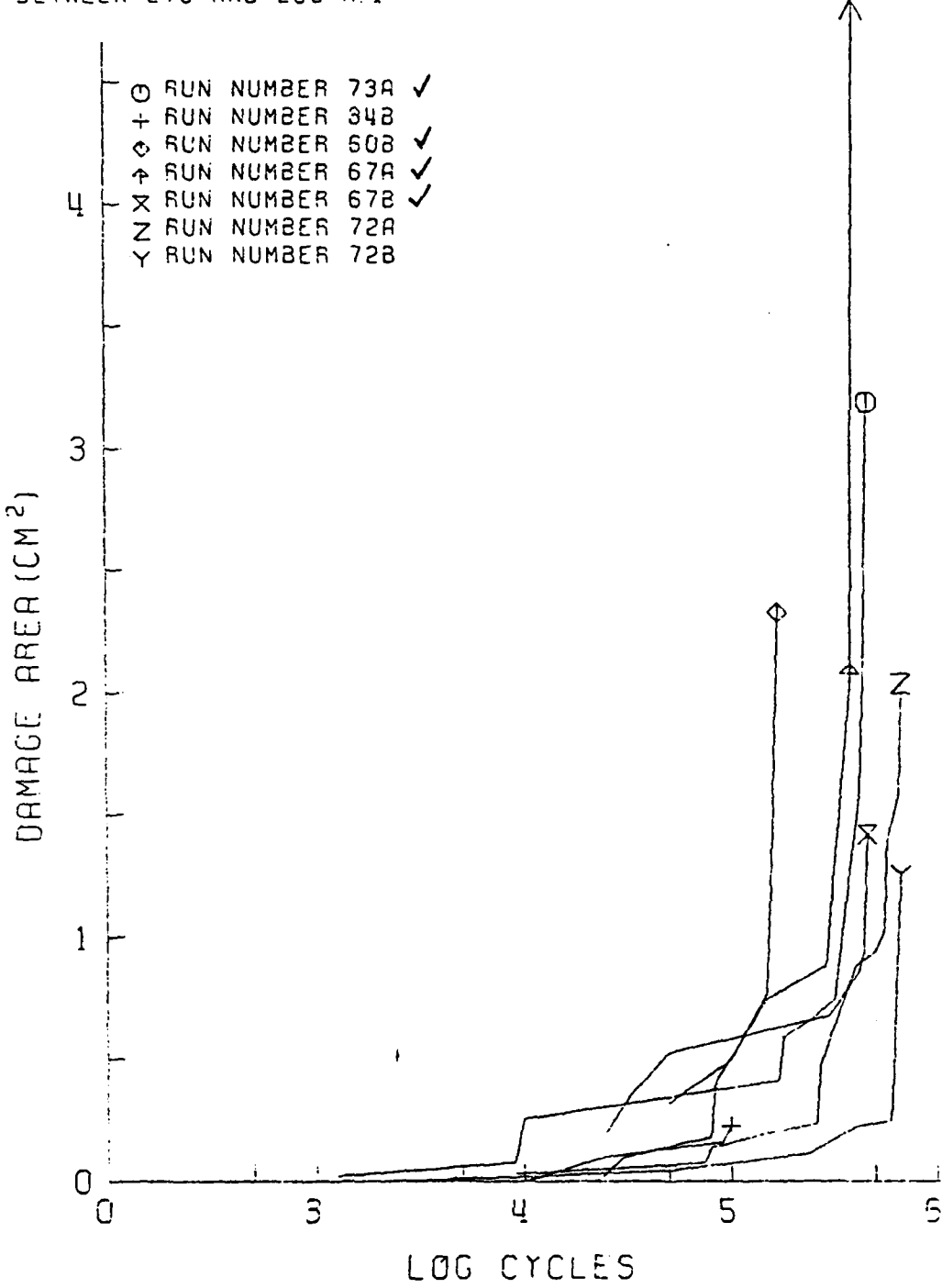
FIGURE 18   DAMAGE AREA VERSUS CYCLES
(±30/0)$_s$ FATIGUE TEST DATA

DATA FOR MAXIMUM COMPRESSIVE LOADS
BETWEEN 275 AND 315 MPa
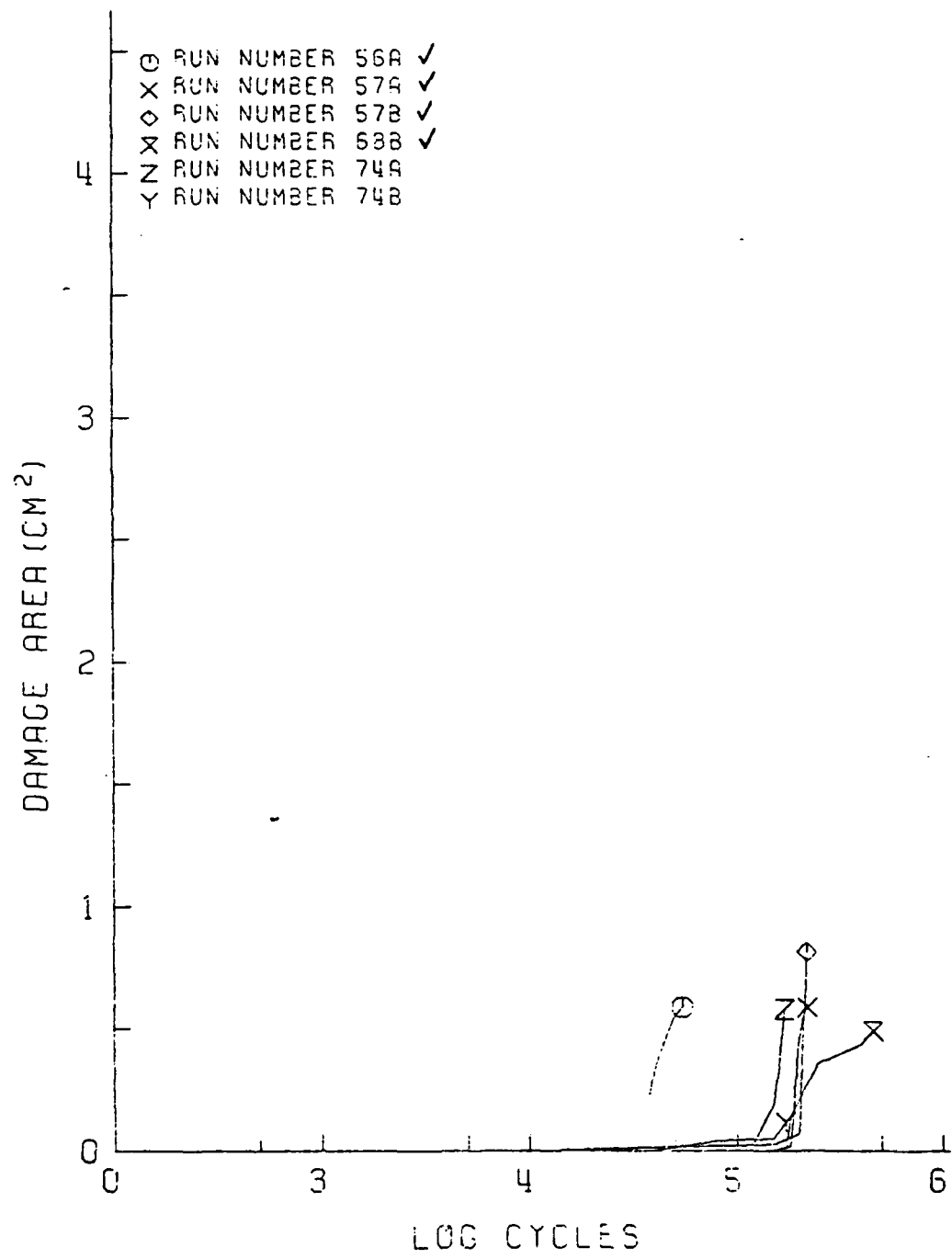
FIGURE **19** DAMAGE AREA VERSUS CYCLES $(0/\pm30)_s$ FATIGUE TEST DATA
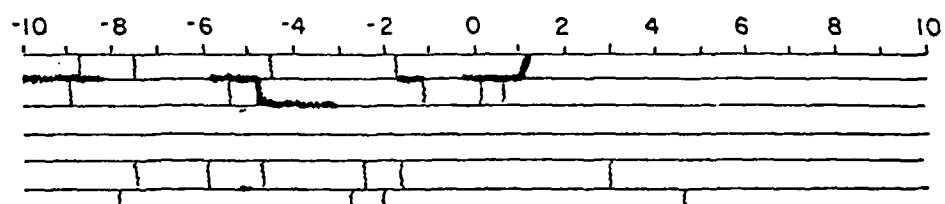
DATA FOR MAXIMUM COMPRESSIVE LOADS
BETWEEN 275 AND 290 MPa

$(\pm 45/0)_s$ Cross Section at ⁻5


Longitudinal Cut 0.5 mm. from Right Edge of Hole

FIGURE 20   FATIGUE DAMAGE IN A
            CROSS SECTION FROM   TEST 34A

$(\pm 45/0)_s$ Cross Section at 1.5
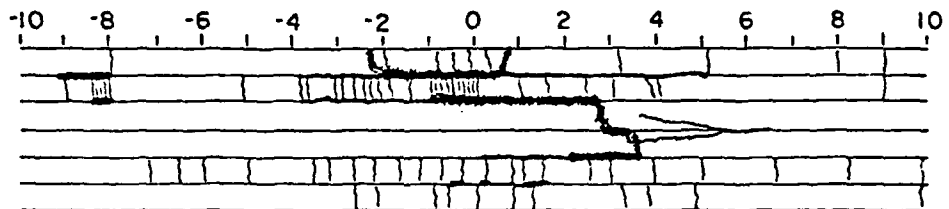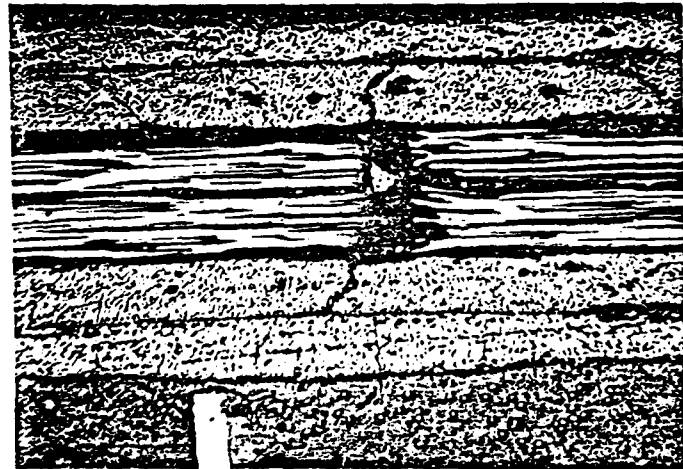

Longitudinal Cut 0.5 mm. from Right Edge of Hole
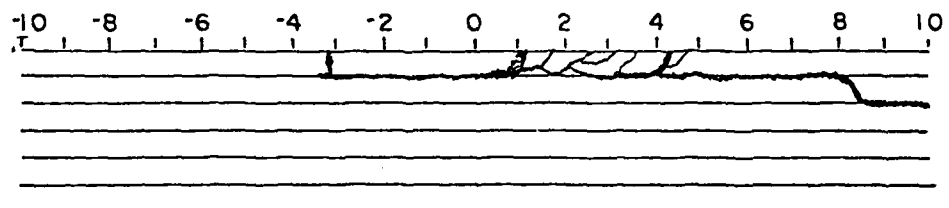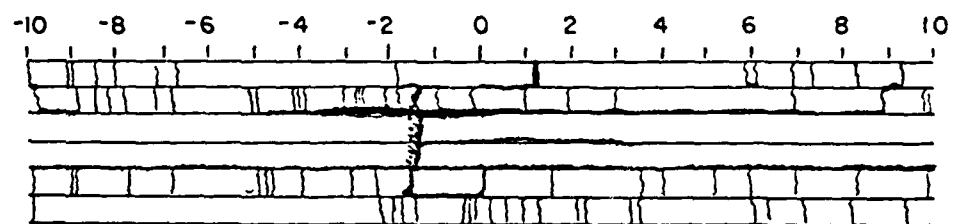
Longitudinal Cut 0.5 cm. from Right Edge of Hole

FIGURE 21   FATIGUE DAMAGE IN
CROSS SECTIONS FROM TEST 63B

(±45/0)   Cross Section at ⁻1.5

Longitudinal Cut 0.5 mm. from Right Edge of Hole

FIGURE 22   FATIGUE DAMAGE IN A
CROSS SECTION FROM TEST 44A

DATE FILMED

-8